Nucleic Acids Research, 2025, **53**, gkae1230
https://doi.org/10.1093/nar/gkae1230
Advance access publication date: 11 December 2024
Molecular Biology

Mechanistic insights into Sindbis virus infection: noncapped genomic RNAs enhance the translation of capped genomic RNAs to promote viral infectivity

Deepa Karki[1], Autumn T. LaPointe[1], Cierra Isom[1], Milton Thomas[1] and Kevin J. Sokoloski[1,2,*]

[1]Department of Microbiology and Immunology, University of Louisville, School of Medicine, Louisville, KY 40202, USA
[2]Center for Predictive Medicine for Biodefense and Emerging Infectious Diseases, University of Louisville, Louisville, KY 40202, USA

[*]To whom correspondence should be addressed. Tel: +1 502 852 2149; Email: kevin.sokoloski@louisville.edu
Present address: Autumn T. LaPointe, Department of Molecular Genetics and Microbiology at the University of New Mexico, Albuquerque, NM, 87131, USA

Abstract

Alphaviruses are globally distributed, vector-borne RNA viruses with high outbreak potential and no clinical interventions, posing a significant global health threat. Previously, the production and packaging of both viral capped and noncapped genomic RNAs (cgRNA and ncgRNA) during infection was reported. Studies have linked ncgRNA production to viral infectivity and pathogenesis, but its precise role remains unclear. To define the benefits of ncgRNAs, pure populations of capped and noncapped Sindbis virus (SINV) gRNAs were synthesized and transfected into host cells. The data showed that mixtures of cgRNAs and ncgRNAs had higher infectivity compared to pure cgRNAs, with mixtures containing low cgRNA proportions exceeding linear infectivity expectations. This enhancement depended on co-delivery of cgRNAs and ncgRNAs to the same cell and required the noncapped RNAs to be viral in origin. Contrary to the initial hypothesis that the ncgRNAs serve as replication templates, the cgRNAs were preferentially replicated. Further analysis revealed that viral gene expression, viral RNA (vRNA) synthesis and particle production were enhanced in the presence of ncgRNAs, which function to promote cgRNA translation early in infection. Our findings highlight the importance of ncgRNAs in alphaviral infection, showing they enhance cgRNA functions and significantly contribute to viral infectivity.

Graphical abstract

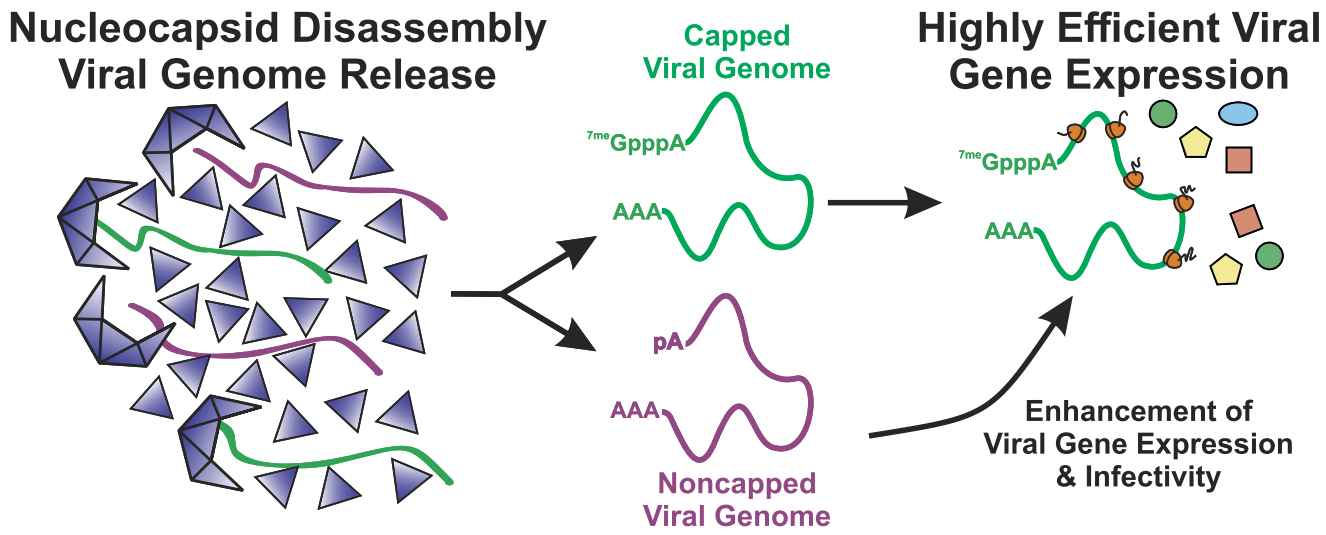

Introduction

The members of the genus Alphavirus, of the family Togaviridae, are a group of small, enveloped, arthropod-borne viruses whose natural cycle of transmission is maintained between vertebrate, reservoir hosts and invertebrate, arthropod vectors (1–4). Alphaviral infection in arthropods is largely asymptomatic resulting in the persistent infection of host cells with negligible effects on their biological functions (5). Nonetheless, infection of vertebrate hosts is characterized by high-titer viremia, rash and fever, and a cellular infection cycle that

Received: June 24, 2024. **Revised:** November 15, 2024. **Editorial Decision:** November 25, 2024. **Accepted:** November 29, 2024

acutely results in host cell death except for several specific cell types, including skeletal muscle and macrophage (6). Based on their clinical symptomology, alphaviruses are categorized as either arthritogenic or encephalitic. The encephalitic diseases that are primarily caused by the New World alphaviruses, such as Venezuelan equine encephalitis virus, Eastern Equine encephalitis virus and Western equine encephalitis virus, are relatively rare despite their capacity to cause periodic outbreaks. Clinically, the encephalitic alphaviruses exhibit high mortality and often result in significant life-altering neurological sequelae such as paralysis and seizures in survivors of clinical encephalitis (7–10). On the contrary, the diseases caused by Old-World alphaviruses, which continually reemerge in Asia, Africa and Americas, such as Chikungunya virus (CHIKV), Ross River virus, Mayaro virus and Sindbis virus (SINV), are associated with non-life-threatening symptoms such as febrile illness with rash and severe arthralgia/arthritis which may sometimes persist for years after the resolution of the primary infectious event (11–14). Due to epizootic spillover, human symptomatic SINV infections in immunologically naïve but otherwise healthy individuals have been reported in northern Europe (Finland, Sweden), Russia and South Africa (15); with Finland reporting the largest SINV outbreak in the EU as recently as 2021 (16). Habitat expansion of vector-competent mosquito species, primarily because of global warming, economic globalization, and human intervention (17,18), has resulted in a global re-distribution of alphaviruses and vector-competent mosquito species resulting in several significant outbreaks in Asia, Europe and the Americas over the last decade (16,19,20). Despite such instances of alphaviral re-emergence, and their clear negative impact on human health during the acute and convalescent stages of infection, there are no clinically approved treatments or antiviral therapies, nor are their safe and effective vaccines that lack reactogenicity to combat alphaviral infections and protect at-risk populations. Recent advances have resulted in the development of new-generation vaccines for several alphaviruses, in particular CHIKV, but as these vaccines continue to exhibit reactogenicity similar to the prior iteration it is unclear as to their efficacy in a broad population (21).

SINV) a prototype species of the genus Alphavirus, has a single-stranded, positive-sense (+) RNA genome ∼11.5 kb in length with a 5′ Type-0 cap structure and a 3′ poly(A)-tail (2,22–24). Upon entering the cell, the viral genomic RNA (gRNA) serves as messenger RNA (mRNA) for translation of the viral replication machinery. The gRNA, containing the first open reading frame (ORF), encodes the four non-structural proteins (nsP1-4) as a polyprotein, which undergoes tightly regulated autoproteolysis to form the viral RNA replication complex which is ultimately responsible for the synthesis of the minus-strand RNA template, from which new viral genomic and subgenomic RNAs are synthesized (25–28). The subgenomic RNA, containing solely the second ORF, encodes the viral structural proteins, which are assembled with viral gRNAs into nucleocapsid cores during the process to release mature viral particles (29–31).

The presence of a Type-0 cap structure on the SINV gRNA enables them to function similarly to cellular mRNAs and use the host translational machinery for viral gene expression. The alphaviral capping reaction is catalyzed by the combined action of the viral nsP1 and nsP2 proteins (32–35). During the viral capping reaction a ^{7me}GMP-nsP1 intermediate is formed by the methylation of a GTP molecule via methyltransferase activity of nsP1 (32,33). Concurrently, a nascently transcribed vRNA bearing a diphosphate moiety is formed by way of hydrolyzing the 5′ β–γ-phosphate bond of the nascent vRNA via the RNA triphosphatase activity of nsP2 (34,35). Finally, the 7meGMP moiety is transferred to the 5‘ end of the 5′ diphosphate vRNA via the GTase activity of nsP1 to form the final Type-0 7meGpppA cap (32).

Although vRNA capping is critical during viral infection to enable the expression of the alphaviral replicase and structural genes, the synthesis of both capped and noncapped gRNAs (cgRNAs and ncgRNAs, respectively) has been reported during vertebrate and invertebrate infections. In addition, these distinct vRNA species have been determined to be packaged into viral particles during viral infection; however, the underlying role of the ncgRNAs synthesized in the host cell and delivered via viral particles to the next host during infection was unclear (36). Using discrete point mutations in the nsP1 protein to modulate viral RNA capping, it was demonstrated that altering capping efficiency negatively impacted viral growth kinetics in tissue culture models of infection. Specifically, as anticipated, increasing the production of the ncgRNAs via reducing the MTase and GTase activities of the nsP1 protein decreased viral titer; however, paradoxically, enhancing the MTase and GTase activities also reduced viral titer despite increased synthesis of the cgRNA species (37,38). Correlating with decreased viral growth kinetics, the plaques formed by the SINV.D355A nsP1 mutant, which has increased capping efficiency, were approximately half the size of plaques produced by the wild type parental SINV strain. Further characterization revealed a strong positive correlation between decreased viral particle production and viral growth kinetics, yet the magnitude of the effect of increased capping efficiency on viral particle production was comparatively much lower than those observed for viral titer (38). Therefore, this observed reduction in viral growth kinetics could not be solely explained by the observed reduction in viral particle production, and an additional deficiency must underlie viral infections where the vRNA species primarily synthesized and packaged into viral particles are cgRNAs. From these observations, it was hypothesized that the ncgRNAs exert an early effect on SINV replication affecting the basal infectivity of the viral particles being produced, and, as a consequence, the infectious potential of the viral population as a whole.

Here in this study, through the use of the aforementioned nsP1 capping mutants, it was confirmed that decreased ncgRNA production negatively impacted the ability of viral particles to initiate infection, thereby resulting in reduced viral titers and the inefficient spread of the infection to neighboring cells. Furthermore, to precisely define the contributions of the ncgRNAs towards viral infection, pure populations of capped and noncapped SINV gRNAs were synthesized, and precisely defined mixtures of these gRNAs were transfected into highly permissive host cells. The data from these efforts demonstrate that the ncgRNAs significantly contribute to infectivity despite being poorly infectious by themselves. Importantly, it was determined that SINV infections significantly benefit from a ‘multi-hit’ kinetics phenomenon involving the delivery of the two vRNA populations (i.e. cgRNAs and ncgRNAs) into the same host cell. Importantly, this benefit of enhanced vRNA infectivity is dependent on the noncapped RNA being viral, indicating that sequence specificity is required for the effect. Subsequent virological analyses to understand the impact of the ncgRNAs at the molecular level

revealed the influence of the ncgRNAs on viral translation and vRNA synthesis/accumulation. Thus, the ncgRNAs contribute meaningfully to vRNA infectivity despite being largely inert. Using a replication-deficient system that harbors a GAA mutation within catalytic triad of nsP4, it was found that the ncgRNAs exert a controlling influence on early replication events through the direct enhancement of incoming cgRNA translation. The enhancement afforded by the ncgRNAs is dependent on their translational inactivity, as modestly restoring the translational capacity of the ncgRNAs abrogated the enhancement of cgRNA function.

Altogether the data obtained from these efforts demonstrate that the ncgRNAs have a distinct molecular role by themselves despite their ultimate biological activity requiring the presence of the cgRNA species. Collectively, these data provide evidence that the ncgRNAs enhance the translational efficiency of incoming cgRNAs, producing a cumulative effect by increasing vRNA replication and facilitating the production of infectious virus particles.

Materials and methods

Tissue culture cells

BHK-21 cells (ATCC CCL-10, VA, USA) used for this study were maintained in Minimal Essential Media (Corning; Catalog #10–009-CV) supplemented with heat-inactivated 10% fetal bovine serum (Corning; Catalog #35–010-CV), 1% penicillin/streptomycin (Corning; Catalog #30–002-CI), 1% non-essential amino acids (Corning, Catalog #25–025-CI) and L-glutamine (Corning; Catalog #25–005-CI). Cells were cultured at 37°C in the presence of 5% CO_2.

Virus generation

Wild-type SINV, SINV.D355A and SINV.N376A strain viruses were generated by electroporation as described previously (39,40). Briefly, 10 μg of *in vitro* transcribed viral RNA was electroporated into ∼2.8×10^6 BHK-21 cells using a single pulse via a Gene Pulser Xcell electroporation system (Bio-Rad). The electroporation condition was 1.5 kV, 25 mA and 200 Ohm. The electroporated cells were transferred to a flask and incubated at 37°C. Following the development of cytopathic effects (usually 24–36 h post-electroporation), the supernatant was collected and subjected to centrifugation for clarification. The clarified supernatant was aliquoted and viral stocks were stored at −80°C for later use.

Plaque formation assay using real-time fluorescence microscopy

BHK-21 cells were grown to 80–90% confluency in a 96-well plate incubated at 37°C under 5% CO_2. The cell monolayers were infected with either SINV.WT or one of the SINV nsp1 mutant viruses expressing the fluorescent protein Green Fluorescent Protein (GFP) or mKate (as described below) over a range of serial dilutions to ensure the formation of evenly spaced single infectious foci. After 1 h of incubation at 37°C, the culture media was removed, and the cell monolayers were washed twice to remove unbound viral particles. The infected cell monolayers were then overlaid with 100 μl of 0.5% agarose containing Minimal Essential Media (MEM). The 96-well plates were then incubated in a BioTek Cytation One Cell Imaging system at 37°C in the presence of 5% CO_2. At regular intervals for a period of 24 h, the whole well was imaged using Brightfield and GFP imaging using a 4× objective.

The montaged images were aligned using the Brightfield image sets to generate a 'stitched' image for further analysis. To determine the relative rate of fluorescent infectious center growth, the images were analyzed via the Gen5 Image + software package using the image-level analyses settings after background subtraction (as determined by autofluorescence in uninfected wells). The total fluorescent area with respect to time was divided by the number of fluorescent foci to determine the mean rate of infectious center growth.

Plasmids and infectious clone construction

Several plasmids and infectious SINV clones were utilized during these efforts. The infectious clones used for the assessment of infectious fluorescent foci, particle production and viral particle specific infectivity were derived from the parental neurovirulent SINV AR86 strain. These infectious clones contained an mKate reporter protein downstream of the capsid protein via a Foot-and-mouth virus 2A protease scheme. These plasmids are referred to as pAR86.mKate (with the corresponding nsP1 mutant, as appropriate). The *in vitro* work, including all liposome mediated vRNA delivery approaches, used Toto1101-derived infectious clones. These include p389, a Toto1101-derived SINV strain that includes a GFP reporter in frame with the nsP3 protein, p389.mCherry and pToto1101.nanoluc, which are identical in construction to the p389 infectious clone with the exception that the GFP reporter has been swapped for mCherry or Nanoluciferase, respectively (36,41). These infectious clones were generated via Gibson assembly of the corresponding coding regions into the SpeI site of the p389 plasmid using Gibson Assembly® HiFi kit (Catalog #GA1100-10; TelesisBio) as per the instruction manual. Similarly, Gibson assembly was also used to insert the PS4 synthetic IRES element (5′-AGGTGGTAGCCG CAAACATAGTTCAATACAAACTTGCTGTCTCGGCGG-3′) immediately upstream of the non-structural ORF start codon in the context of the wild type 5′UTR (42). All the synthetic DNA fragments of coding regions used to generate these clones were obtained from Genewiz (now Azenta NJ, USA). Also included in these studies were a series of derivative plasmids from each of the three Toto1101-derived infectious clones, which include either a GAA point mutation in the catalytic triad of the nsP4 protein, and/or the PS4 synthetic IRES element. These plasmids were generated using site-directed mutagenesis via the Q5 Site-Directed Mutagenesis Kit (Catalog #E0554). Briefly, the parental plasmids were polymerase chain reaction (PCR) amplified with high-fidelity Q5 DNA polymerase using primer sets- p389.GAA.F (5′-CGCAAACACATACATGG AGTAGTATC-3′) and p389.GAA.R (5′-GCGCCAATGAACGCTGCACATCTG-3′) according to the manufacturer's instructions to ablate the catalytic triad of nsP4.

All plasmids were fully sequenced and validated prior to continuing with their use in the described assays. Plasmid maps and sequences are fully available upon request.

Quantification of viral particle production and infectivity

To determine the quantity of total viral particles produced during infection, BHK-21 cells were infected with either WT AR86 SINV or one of the AR86 SINV nsp1 capping mu-

tant viruses at a Multiplicity of Infection (MOI) of 10 Plaque Forming Units (PFU)/cell and incubated at 37°C in the presence of 5% CO_2. At 24 hpi, the supernatant was collected and clarified via centrifugation. The total viral particle concentrations were quantified using quantitative reverse transcription-PCR (qRT-PCR) as previously described (43). Briefly, 5 μl of supernatant was used as the template for reverse transcription using OneScript Plus Reverse Transcriptase (Catalog #G237, Abm) as per the manufacturer's instructions. The resulting cDNA was used as input for the quantification of vRNA species via qRT-PCR using the method and primers as previously described (36,44).

To determine the infectious potential of the viral particles, the viral titers of the samples from above were quantitatively assessed. Briefly, standard plaque assays were performed on the supernatants collected at 24 hpi to determine the number of infectious particles per infectious unit as described previously (39). The viral specific infectivity was then determined as the ratio of the total number of particles per ml, as quantified by qRT-PCR, to the corresponding infectious units per ml, as measured by standard plaque assays (36,44).

Invitro transcription and *in vitro* vRNA capping method

Linearized templates for *in vitro* transcription of vRNA were prepared by digesting 4 μg of the infectious clone plasmids with the restriction enzyme XhoI (New England Biolabs). The linearized plasmid was purified by using Phenol:Chloroform extraction followed by precipitation in Ethanol and then resuspended in nuclease-free water. To generate pure populations of ncgRNAs, *in vitro* transcriptions were performed, where 1 μg of linearized plasmid was used as a template for transcriptions with SP6 RNA polymerase (Catalog #E2070S; New England Biolabs) in a total volume of 50 μl containing 5 mM of each rNTP (ATP, CTP, UTP and GTP) according to the manufacturer's instructions. After the *in vitro* transcription reaction, the uncapped RNAs were purified using an RNA Cleanup Kit (Catalog #T2030S; New England Biolabs) as directed by the manufacturer. The transcribed uncapped RNAs were post-transcriptionally capped using the Vaccinia Capping System (Catalog#M2080S; New England Biolabs). Following capping, the reaction product was purified using the phenol:chloroform method to obtain populations of pure capped RNAs matched to their noncapped inputs. The quality of the capped and noncapped RNAs were tested using 0.8% agarose gel electrophoresis and RNA concentration was measured using a NanoDrop Microvolume Spectrophotometer (Catalog #ND-ONE-W; ThermoFisher Scientific).

Analysis of vRNA capping efficiency by the vaccinia capping enzyme system

The quantitative assessment of *in vitro* RNA capping efficiency was performed using acrylamidophenylboronic acid (APB) gels as previously described (45,46). Briefly, the *in vitro* synthesized capped and noncapped RNAs were cleaved by a vRNA-specific 10–23 DNAzyme to generate smaller fragments before performing gel-electrophoresis. In the cleavage assay, a target specific 10–23 DNAzyme oligonucleotide (5′-ACAAACGGAGGCTAGCTACAACGATCTGGGGGT C-3′) (11 μM) was annealed with 2.5 μg of *in vitro* transcribed RNA product by heating the mixture to 85°C for 5 min, followed by slow cooling to 30°C. After annealing, the reaction mix was exposed to Tris HCl (pH 7.5; 500 mM), and MgCl2 (100 mM) and incubated at 37°C for 2 h. The reaction was terminated by adding ethylenediaminetetraacetic acid (to a final concentration of 4 mM) and then the cleaved products were purified using Phenol:Chloroform and ethanol precipitation. The cleavage product was diluted with RNA-binding dye and denatured at 90°C for 30 s, followed by on ice for 30 s. The sample was then separated using polyacrylamide gel containing 5% acrylamide and 5% APB in 7 M urea and 0.1 M Tris-acetate was used as a running buffer. The gel was stained with ethidium bromide and visualized using the UVP Bioimaging System (AnalytikJena). The bands of RNA were selected on the basis of size and analyzed using ImageJ software. The total intensity of the capped and noncapped RNAs were quantified and compared to quantify the capping efficiency.

Transfection of cgRNAs and ncgRNAs

BHK-21 cells were transfected with cgRNAs and ncgRNAs at different ratios using Lipofectamine MessengerMAX Transfection Reagent (Catalog #LMRNA001; ThermoFisher Scientific). The transfections were performed under various conditions as specified in the text and figure legends, and generally were as follows:

(i) *Co-delivery approach*: The mixtures of vRNAs transfected via liposome delivery were created by mixing capped and noncapped vRNAs at the corresponding ratios; 100:0, 80:20, 60:40, 40:60, 20:80 and 0:100 (capped-to-noncapped) resulting in a final concentration of 100 ng. The RNA-lipid complexes were generated using the following conditions (described as a per well basis): 0.2 μl of Lipofectamine™ MessengerMax™ Transfection Reagent (Invitrogen) was diluted in 5 μl of Opti-MEM (Gibco) medium and was incubated for 10 min at room temperature (RT). The diluted Lipofectamine complexes were mixed with the premixed RNA solutions containing 100 ng of RNA diluted in 5 μl of Opti-MEM medium. The co-transfection mixture was incubated for 5 min at RT to allow the final RNA-liposome complex to form. Afterwards, 5 μl of the RNA-lipid complexes were added to BHK-21 cells seeded in a 96-well plate which contained 45 μl of fresh medium.

(ii) *High multiplicity independent delivery approach*: The RNA-liposome complexes containing either cgRNAs or ncgRNAs were prepared independently as described above. In this assay format, the Lipofectamine complexes were separately added to form the different ratios of capped or noncapped RNA, and subsequently mixed before administrating into the cells.

(iii) *Low multiplicity independent delivery approach*: Essentially identical to the above independent delivery conditions; however, the transfection mixtures were diluted 1:4 via the addition of Optimem media after the formation of the liposome complexes but before mixing and adding the complexes to the cells.

For all conditions, mastermixes were used to reduce well-to-well variability. The transfected cells were incubated at 37°C in the presence of 5% CO_2 for 3 h prior to the addition of NH_4Cl (40 mM) to block secondary infection and further incubated under the conditions described above. At 24 h post-transfection (hpt), the samples were imaged as described below.

Quantitative assessment of RNA liposome encapsulation

To determine the relative efficicency by which the cgRNA and ncgRNA species were incorporated into liposomes prior to transfection, a dye-exclusion assay was performed. Briefly, liposomes were generated as described above and after formation SYBR Green II RNA dye was added. After incubation for 20 min the amount of unencapsulated RNA was determined via the detection of flourescence at 520 nm after excitation at 497 mm. The total input RNA concentrations were determined using identically formed liposomes treated with Triton X-100 detergent (at a final concentration of 0.05%). The overall encapsulation efficiency was determined by comparing the unencapsulated signal to the input signals after the determination of absolute concentrations using standard curves prepared and ran in parallel.

Quantification of vRNA infectivity by fluorescent microscopic imaging

To evaluate the vRNA specific infectivity of the mixtures of cgRNAs and ncgRNAs, fluorescent protein expression was quantified using the BioTek Cytation One Cell Imaging platform. Briefly, 24 hpt, the tissue culture plates were loaded into the Cytation One instrument and imaged using Brightfield, GFP and/or Red Fluorescent Protein (RFP) filter cube sets to detect expression of the respective fluorophores. The focal plane was maintained during imaging using the Laser Autofocus module trained at the cell monolayer for each plate independently. For these assays, the entire well areas of the target wells were imaged via the capture of multiple images per well with a 4× objective, with the final image for analysis consisting of a 'stitched' image generated via the alignment of the Brightfield data. Background fluorescence detection, to eliminate the detection of false positive events or artifacts, was determined by way of calculating the mean intensity of uninfected/untransfected cells. After background removal, the number of fluorescent-positive cells was determined using the cell-level analyses functions of the Gen5 Image + software package. Regardless of mean or maximum fluorescent intensity, any element larger than 10 μm^2 in area and >5000 arbitrary units of intensity were counted as positive events. To determine vRNA specific infectivity, the number of positive cells per well was quantified per μg of vRNA transfected.

Evaluation of vRNA replication capacity/selection by analysis of fluorescent gene expression

To quantitatively assess the ability of the vRNA cargos to undergo replication, BHK-21 cells grown to 80–90% confluency in 96-wells plates were transfected with premixed vRNA-liposome complex mixtures developed using the 'co-delivery' approach; however, the vRNA cargos contained different fluorophores, specifically capped-RFP and noncapped-GFP vRNAs were used, and vice versa to ensure no indirect impacts of the fluorophore reporters. As previously described, at 3 hpt, NH_4Cl (40 mM) was added tothe incubation medium, and the transfected cells were further incubated for 24 h at 37°C. After 24 hpt, microscopic images of the infected cells were taken in bright and fluorescence mode using BioTek Cytation One Cell Imager. The resulting image was utilized to quantify the expression of GFP, RFP and G&RFP reporter-positive cells, as described above.

Quantification of viral titers by TCID50 assays

The infectious virus particles produced during transfection and their parental derivation, via GFP and RFP expression, were quantified by determining the tissue culture infectious dose (TCID50) for each sample. Briefly, a confluent monolayer of BHK-21 cells in 96-well plates at a density of 3.2×10^4 cells/well was transfected with a premixed vRNA-liposome complex containing capped-RFP and noncapped-GFP vRNA in the presence or absence of NH_4Cl as described above for the assessment of replication capacity. After 24 hpt, the tissue culture supernatant was collected and stored at 4°C. For the quantification of infectious viral titer generated post-transfection, TCID50 was performed in 384 wells plates seeded with BHK-21 cells. The obtained results were then converted to PFU per unit volume/mass by way of calibrated TCID50 assays using standardized samples.

Quantification of vRNA synthesis and accumulation

To quantify the genomic, subgenomic and negative-sense SINV vRNAs, BHK-21 cells were transfected with different ratios of capped and noncapped vRNA containing the nanoluciferase gene within the nspP3 protein by the co-delivery mechanism as described above. At the indicated time points the tissue culture supernatants were removed, and the cells were washed twice with phosphate-buffered saline (PBS) (1×) before harvesting in TRIzol reagent (Catalog #15596026; Invitrogen). Total RNA was extracted using a KingFisher™ Duo Prime Purification System (Catalog #A39956; ThermoFisher Scientific) as described by the manufacturer using Direct-zol-96 MagBead RNA extraction kit (Catalog #R2103; Zymo Research).

Equal amounts of total extracted RNAs were used as the template for reverse transcription using OneScript Plus Reverse Transcriptase (Catalog #G237, Abm) as per the manufacturer's instructions. The resulting cDNA was used as input for quantification of individual vRNA species using qRT-PCR and primers as described previously (38). Briefly, a cocktail of specific RT primers based on the intended amplification targets was applied to detect different vRNA species. To detect the positive-sense RNA species, the RT primer cocktail consisted of nsP1, E1 and 18S rRNA reverse primers; to detect the minus-strand RNA species, the RT primer cocktail consisted of nsP1 forward and 18S rRNA reverse primers. The total positive sense vRNA was quantitatively assessed via amplification with the primer set of E1. The viral gRNA was determined using the nsP1 primer set. The quantity of subgenomic RNA was calculated as: Total positive sense RNA (E1) – Total viral gRNA (nsP1) (43). To amplify minus-strand, the nsP1 primer set was used. All vRNA quantities were normalized to the abundances of vRNAs present at 2 hpt for the 0% cgRNA condition.

Quantification of viral gene expression via nanoluciferase assays

To quantify genomic vRNA translation during transfection, BHK-21 cells were seeded into 96-well plates with 3.2×10^4 cells/well one day before transfection,. The tissue culture monolayers were then transfected with different ratios of capped and noncapped vRNA containing the nanoluciferase gene within the nsP3 protein via a co-delivery mechanism as previously described. After incubation at the indicated time post-transfection, the tissue culture supernatants were care-

fully removed and replaced with 100 μl of OptiMeM (Catalog #31985070, Gibco) supplemented with Furimazine (Catalog #AOB36539; AOBIOUS) at a concentration of 10 μM. The nanoluciferase activity was recorded using a BioTek Cytation One Cell Imaging microplate reader after brief incubation of 2 min at RT (44).

To quantify nanoluciferase expression in real-time, the above nanoluciferase assay was performed on the transfected cells using Nano-Glo Luciferase Live Cell Assay System (Catalog #N1110; Promega) in 96-well plate format according to manufacturer's instructions. Briefly, at 80–90% confluency, the tissue culture supernatant was removed, and the cells were washed with PBS (1×). Then the cells were supplemented with OptiMeM (Catalog#31985070; Gibco) containing Nano-Glo Luciferase Assay Reagents before transfecting the cells via a co-delivery mechanism. After 3 min, luciferase signals were measured immediately using a BioTek Cytation One Cell Imaging microplate reader every 2.5-min intervals for 1.5 h.

The resulting data was used to calculate non-linear regressions to enable comparative analysis of the different transfection conditions including confidence interval comparisons to determine statistical significance. Briefly, the underlying data was assessed using GraphPad Prism (version 10.2.0) non-linear regression analyses concentration versus response – variable slope (four parameters) with the bottom parameter constrained to zero. To determine the impact of the ncgRNAs to the rate of cgRNA translation, the data set was truncated to the time corresponding to the inflection point of the non-linear regression above, and a new non-linear exponential growth regression analysis was performed to enable comparison of the rate of translational activity (as per the slope of the exponential growth regressions). For the exponential non-linear regression analyses, the expected values were determined via calibrating the slope of the equation to the relative contributions of the cgRNA and ncgRNA components as determined by their pure populations (i.e. the expected slope of the 60% sample consisted of the sum of 60% of the 100% capped and 40% noncapped rates).

Quantification of concurrent infection – transfection assays

To assess whether the addition of exogenous viral ncgRNAs could enhance viral particle infectivity a concurrent infection – transfection approach was devised and employed. Specifically, equal amounts of BHK-21 cells were exposed to SINV.WT, SINV.D355A or SINV.N376A at multiplicities of exposure (MOEs) of either 300 or 30 particles per cell in a minimal volume of media. Concurrently during the absorption period, the cells were transfected with liposomes containing solely SINV ncgRNA or non-specific RNAs prepared as described above. To enable downstream assignment of the infectious event the viral particles and the ncgRNAs encoded different fluorophores, GFP and mCherry, respectively. After 1 h the inoculum/transfection media was removed from the cells and whole media supplemented with ammonium chloride to prevent cell-to-cell spread of the infection was added. The cells were incubated as normal for 24 h prior to flourescence imaging and quantification, as described above.

The number of reporter positive infected cells were numerated. Each virus was internally normalized to the corresponding non-specific transfection condition as the infectivity of the viral particles differs between the SINV mutants. In addition to allowing for direct comparisons this normalization process also controls for any direct or indirect impacts of lipid transfection on the infection process.

Statistical analyses

Unless otherwise indicated in the figure legend, a minimum of three independent biological replicates were used for all quantitative measurements. Data are shown as quantitative mean ± standard deviation (SD) with SD being represented by the error bars. As previously described, variable bootstrapping was used to perform statistical analysis of comparable samples, where appropriate (39). Statistical significance was determined using Student's *t*-test, with statistical significance set at P-value < 0.05. When conducting multiple comparisons, such as those depicted in Figures 5 and 6, the Benjamini–Hochberg procedure was used to correct for false discovery during multiple comparisons. The statistical significance of the non-linear regression analyses was determined via plotting the 95% confidence interval, in that if the shaded areas of the non-linear regressions were independent and non-overlapping, they were different by a P-value of at least 0.05. The exponential growth phase presented in Figures 7C and 8C were statistically assessed using area under the curve (AUC) analysis to distinguish the differences in the cumulative ratio of Observed to Expected for the nanoluciferase activity.

Results

Altering the capping of SINV viral RNAs negatively impacts viral particle infectivity

Previously it was demonstrated that altering capping efficiency negatively impacted viral growth kinetics and plaque formation through an unknown mechanism but presumably related to cell death (38). From these studies it was determined that altering capping efficiency negatively impacted viral particle production; however, the magnitude of effect observed was not wholly explanative as to the net decrease of viral growth kinetics, requiring further assessment to determine the underlying mechanism of attenuation. To further examine this phenomenon, real time fluorescent imaging was used to quantitatively assess viral plaque formation. Briefly, BHK-21 cells were infected with wild type SINV (SINV.WT) or one of the SINV nsP1 mutants, D355A (SINV.D355A) or N376A (SINV.N376A), expressing GFP in frame with nsP3. After infection, the cell monolayers were then overlaid with agarose, and finally, the spread of fluorescent foci was imaged until 24 hpi over intervals of 1 h. Representative animated image series of SINV.WT, SINV.D355A and SINV.N376A infections may be found in the supplemental materials accompanying this manuscript as Supplementary File 1. As expected, SINV.WT formed large infectious centers by 24 hpi. In contrast to SINV.WT, the infectious centers produced by the nsP1 mutants SINV.D355A and SINV.N376A (which increase and decrease capping efficiency, respectively) were reduced in area, as indicated by the relative differences in the mean diameters of their infectious centers (Figure 1A). Specifically, the infectious centers of the SINV.D355A and SINV.N376A nsP1 mutants were approximately one-half and three-fourths of the size of those produced by SINV.WT, respectively at 24 hpi. On the whole a similar trend of a lag phase followed by exponential growth starting by ∼12 h was observed for all SINVs tested; yet the overall exponential growth was less pro-

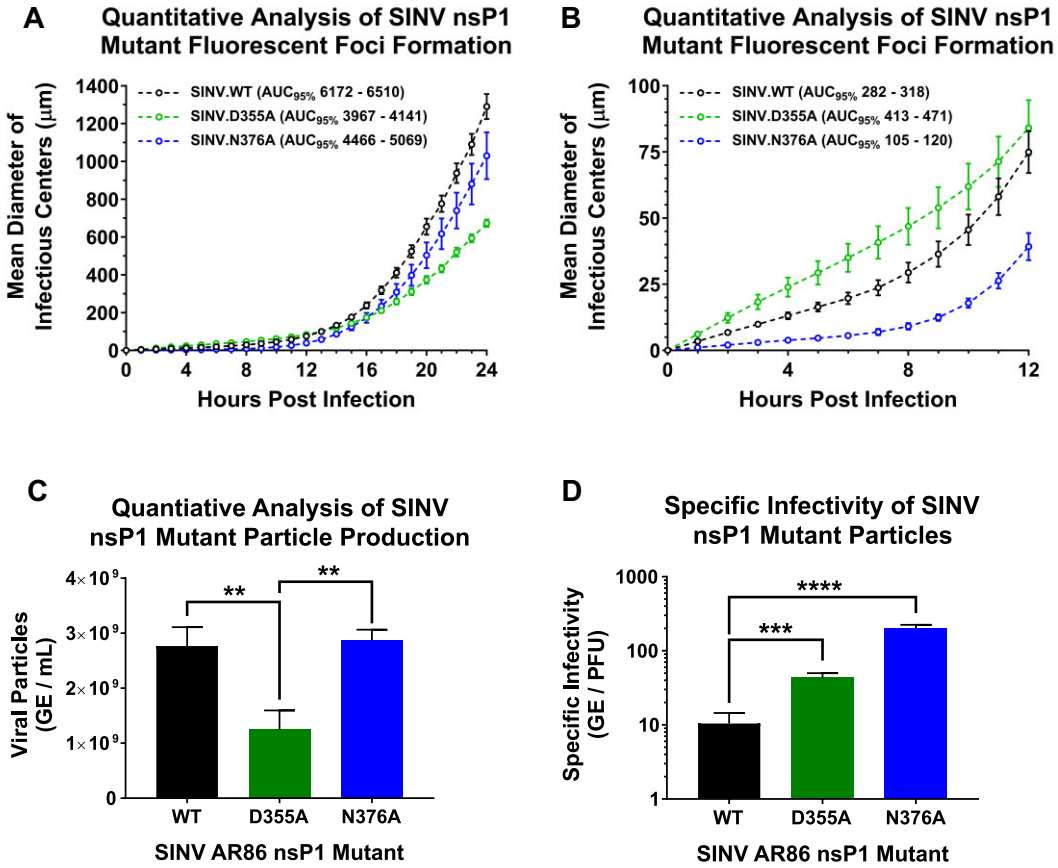

Figure 1. Altering nsP1 capping activity negatively impacts viral growth in tissue culture cells via the production of poorly functional viral particles. (**A**) Highly permissive BHK-21 cells were infected with either SINV.WT, SINV.D355A, or SINV.N376A and viral plaque growth was monitored using real time fluorescence microscopy for a 24-h period. (**B**) Identical to panel (A), with the exception that the Y- and X-axis have been adjusted to focus on the early stages of viral infection. (**C**) SINV particle production was evaluated via standard curve qRT-PCR to determine the production of, in terms of genome equivalents per ml (GE/ml), viral particles up to 18 hpi. (**D**) Comparative analysis of viral particle specific infectivity as determined by the ratio of total particles per infectious unit, as reported as GE/PFU. All quantitative data shown is the mean of at least three independent biological replicates, with the error bar representing the SD of the means. For the data presented in panels (A) and (B), statistical significance of at least *P*-value of < 0.05 is indicated by non-overlapping 95% confidence intervals of the AUC values, as reported in the figure legend. Statistical significance in panels (C) and (D), as indicated by ** and ****, represent *P*-values of <0.01 and <0.0001 as determined by one-tailed Student's *t*-test, respectively.

nounced for the SINV.D355A mutant, as the rate of growth and the cumulative average size of the infectious center were less than those observed for either SINV.WT or SINV.N376A. Interestingly, closer inspection of the infections at times earlier than 12 h revealed a notable difference in the mean diameters of the fluorescent foci formed by the SINV.D355A mutant, which were comparatively larger than those formed by SINV.WT or SINV.N376A (Figure 1B). This difference can likely be attributed to the enhanced translation previously reported for the SINV.D355A mutant resulting in the pronounced detection of GFP-positive cells.

Overall, the plaque formation data revealed an inefficient spread of infection to neighboring cells when capping efficiency was increased. This led to the hypothesis that altering capping efficiency affects the production and infectious potential of the progeny viral particles. To quantitatively assess the total number of viral particles generated during infection, BHK-21 cells were infected with SINV.WT or the SINV nsP1 capping mutants for 24 h followed by the collection of tissue culture supernatants containing the released extracellular viral particles. As SINV is a positive-sense RNA virus, viral particle quantities may be accurately represented by the number of gRNA equivalents per ml (GE/ml). As shown by Figure 1C, the production of viral particles was decreased ∼3-fold for infections of SINV.D355A relative to SINV.WT, while the total number of particles produced by the SINV.N376A mutant were comparable to that observed during SINV.WT infections. While a reduction in particle production correlated with the observed defects in viral titer and plaque diameter, the magnitude of the quantitative differences between SINV.D355A and SINV.WT was not fully explanative as to the general deficiencies associated with the D355A nsP1 mutation. As differences in viral infectivity also have the potential to alter viral growth kinetics and plaque formation, the specific infectivity of SINV.WT, SINV.D355A and SINV.N376A were quantitatively evaluated. In this instance, viral infectivity is defined as the ratio of the total number of viral particles (as measured by GE/ml, as per above) to the number of infectious particles (as per PFU/ml) as determined by plaque assay. A higher particle-to-PFU ratio signifies that more viral particles are required to constitute a single infectious unit, thereby signifying that the capacity of the virus particles to initiate infection is reduced, and vice versa. As depicted in Figure 1D, reducing the capping efficiency, as per the SINV.N376A

mutant, negatively impacted viral infectivity relative to wild type SINV by a magnitude of ∼20-fold. Furthermore, a significantly higher particle-to-PFU ratio for the SINV.D355A mutant relative to SINV.WT was observed, indicating that, counterintuitively, the infectious potential of the nsP1 mutant with greater capping efficiency was ∼5-fold less than that of SINV.WT.

Taken together, these data show that increasing or decreasing the capping efficiency of the SINV nsP1 protein, and by extension, the production of cgRNAs and ncgRNAs negatively affected the functional capacity of the viral particles resulting in decreased titer. Nonetheless, while increasing the production of ncgRNAs as per the nsP1 N376A mutant is easy to reconcile with decreased infectious capacity, precisely how increasing nsP1 capping efficiency, which in turn reduces the production of the ncgRNAs, results in poor infectivity is unclear.

Specific viral RNA infectivity correlates with cgRNAs in a non-linear manner

The observation that decreasing ncgRNA production negatively impacted viral-specific infectivity was confounding, as the ncgRNAs themselves have been previously associated with noninfectious viral particles or particle populations with low specific infectivity. These data revealed a need to better understand the infectious potentials of the individual gRNA species in the cellular host environment to define the molecular consequences of the ncgRNAs.

To assess the underlying infectious potentials of the cgRNAs and ncgRNAs, an *in vitro* transcription system was utilized to generate pure populations of capped and noncapped SINV gRNAs. Briefly, and as depicted in Figure 2A, *in vitro* transcriptions involving full-length SINV cDNA infectious clones encoding a GFP reporter protein internal to the nsP3 protein were used to generate a population of purely ncgRNAs. To generate type-0 cgRNAs from these *in vitro* transcribed ncgRNAs, a Vaccinia Capping Enzyme (VCE)-based approach was used to add the 5′ cap structure prior to purification of the *in vitro* transcribed vRNAs.

Studies on the VCE system have suggested that the functional capacity of the VCE, irrespective of the mRNA length, to cap *in vitro* transcribed RNA is nearly 100% (47–49). Nonetheless, the capping efficiency of the VCE-based approach was independently validated as the production of pure populations of cgRNAs and ncgRNAs is critically important to the downstream efforts designed to assess the molecular importance of the ncgRNAs. Hence, to validate that the above approach generated pure populations of cgRNAs, the electrophoretic mobility of the gRNAs was assessed using boronate-agarose gel electrophoresis after cleavage of the full-length gRNAs via a 10–23 DNAzyme approach to enhance the resolution of the RNA species (45,46,50). As shown in Figure 2B, this approach enables the detection of RNAs that are capped through the altered migration of RNA species containing *cis*-diol moieties. Consistent with previous reports,the capping efficiency of the VCE system was observed to be ∼100% (Figure 2C) (47–49). Taken together, these data confirm the utilized approach consistently results in the production of a nearly pure cgRNA population.

As the data stemming from investigations using the SINV nsP1 mutants are highly suggestive that viral infectivity is linked to capping efficiency in a perplexing manner, a

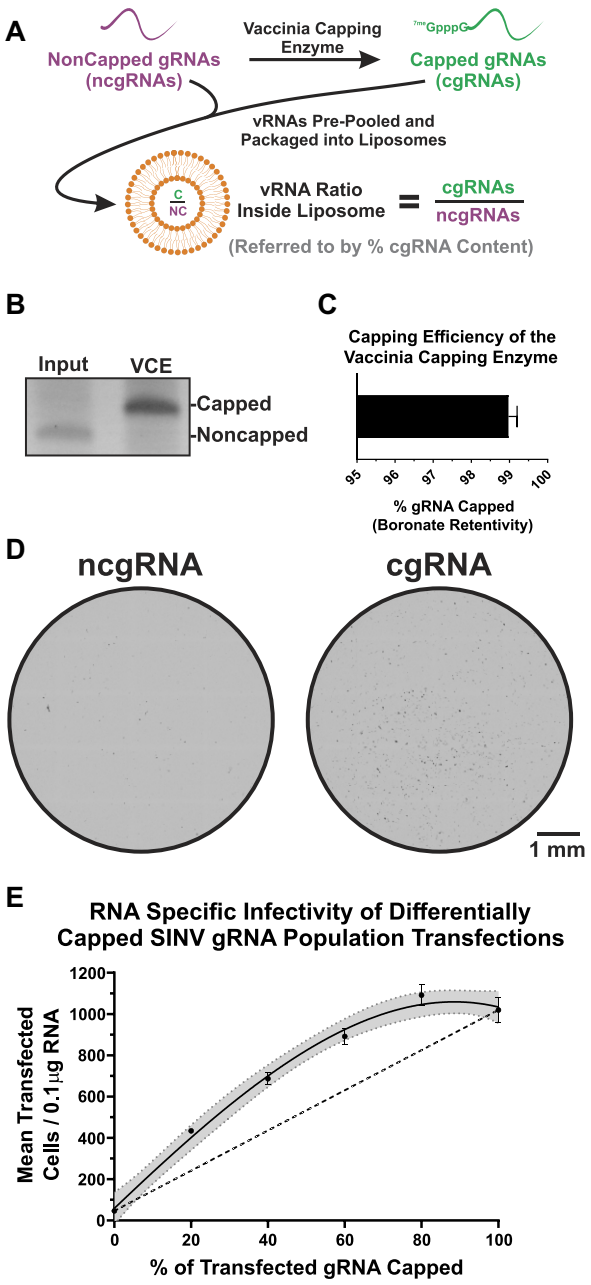

Figure 2. Co-transfection of capped and noncapped SINV gRNAs enhances RNA specific infectivity. (**A**) A schematic of the process used in this study to generate bona fide populations of purely capped and noncapped SINV gRNAs. (**B**) Boronic acid agarose gel analysis of ncgRNAs and cgRNAs produced during these studies. Data shown is representative of multiple independent replicates. (**C**) Quantitative analysis of cgRNA population purity, as determined by densitometric analysis of boronic acid agarose gel electrophoreses assessments. (**D**) Representative images of single 96-wells transfected with pure populations of SINV ncgRNAs or cgRNAs encoding a GFP reporter. For clarity the images have been inverted to produce dark spots on a lighter background to aid in visualization. (**E**) Quantitative analysis of vRNA specific infectivity in the highly permissive BHK-21 cell line after transfection by liposomes containing mixtures of cgRNA and ncgRNAs. After incubation in the presence of ammonium chloride, viral infection was quantified via fluorescent reporter detection at 24 hpt. Data shown is the mean of six independent biological replicates, with the error bar representing the SD of the means. The solid line indicates the non-linear regression of the observed data, and the shaded area indicates the corresponding 95% confidence interval. The dashed line represents a linear model representing the purely cgRNA and ncgRNA populations.

liposome-mediated transfection approach was used to determine the basal rates of infectivity for pure cgRNAs, ncgRNAs, and complex mixtures of the same. Specifically, for the co-delivery approach outlined in Figure 2A, different ratios of *in vitro* transcribed full-length cgRNAs and ncgRNAs encoding the fluorescent reporters were mixed prior to the assembly of liposomes using cationic lipid complexes. Importantly, the range of liposomes generated during these studies varied solely in their composition, as the overall amount of RNA being complexed into liposomes and delivered to host cells remained constant, and the efficicency by which the cgRNAs and ncgRNAs were packaged into liposomes were equivalent (Supplemental Figure S1). To assess the contributions of the cgRNAs and ncgRNAs to specific infectivity, the pre-formed liposome complexes consisting of different ratios of the cgRNAs and ncgRNAs were transfected into highly permissive BHK-21 cells. At 3 h post-transfection (hpt), the media was supplemented with NH_4Cl to block secondary rounds of infection, enabling the detection of successful infection of the host cells receiving the liposome complexes via the detection of the fluorescent protein reporter following viral replication and gene expression. Representative images of transfections of pure SINV ncgRNA and cgRNA transfections are shown as Figure 2D, and higher magnification micrographs may be found as Supplemental Figure S2. As shown by Figure 2E, the number of cells expressing the fluorescent reporter protein was quantitatively analyzed using fluorescent imaging at 24 hpt. In Figure 2E, the solid line represents a centered cubic non-linear regression of the observed data represented by the mean and SD for each ratio of cgRNA:ncgRNA (expressed as a function of the percentage of gRNA capped within the liposome). The shaded area represents the 95% confidence interval of the non-linear regression, and the dashed line represents the expected linear relationship between the infectivity and the presence of a 5′ cap structure based on the function of cgRNAs. A strong positive correlation between the viral RNA infectivity and the presence of cgRNAs was observed; however, the relationship was found to be non-linear, as the RNA infectivity of mixed ratios was well above the anticipated values of the linear model of infectivity. Moreover, the infectivity of the gRNAs shifts downwards as the ratio of cgRNA to ncgRNAs approaches totality.

Together, these data show that cgRNAs and ncgRNAs are acting together and that the cgRNAs benefit functionally in the presence of ncgRNAs to elicit better infectivity. Nonetheless, the precise means by which the ncgRNAs enhance RNA infectivity via the function of the cgRNAs remains unknown.

Enhanced vRNA infectivity depends on the co-delivery of the virally derived ncgRNAs

As the data obtained from the co-delivery method utilized above suggests that the concurrent transfection of cgRNAs and ncgRNAs into the same host cell may be necessary to exhibit their function, it was important to determine the parameters underlying the enhancement of vRNA infectivity. Integrated co-transfection involving premixing nucleic acids before adding transfection reagents maximizes the efficiency by which nucleic acids are concurrently delivery into the same cell; however, the independent preparation of liposome complexes containing a single vRNA type, coupled with simultaneous transfection enables the assessment of the importance of concurrent delivery of the ncgRNA and gRNAs to the same host cell (51,52).

Therefore, to better understand the requirements for the enhancement of RNA infectivity imparted by the ncgRNAs, a similar vRNA transfection experiment to that described earlier was performed except instead of premixing the vRNAs prior to forming liposome complexes, separate liposome complexes of solely cgRNAs or ncgRNAs were produced independently and then briefly mixed to the desired ratios immediately prior to transfection (Figure 3A). When the relative infectivity of these independent, single-liposome complex transfections was examined, a similar profile to that of the co-delivery model was observed despite a general reduction inthe overall number of infectious events observed (Figure 3B). Indeed, these data show that altering the basal likelihood of co-delivering the two vRNAs species into the same cell reduces the infectious potential; however, vRNA infectivity still follows a non-linear relationship. This non-linearity can be readily explained by the independent yet concurrent delivery of the cgRNAs and ncgRNAs as the high relative quantities of the vRNA liposome complexes transfected closely mimics the co-delivery onto the same cell achieved by a single-liposome complex system (51). In short, as the overall concentration of independently formed liposome complexes was sufficient to drive multi-hit kinetics, a similar phenotype to co-delivery was observed.

While concurrent delivery of independently prepared liposomes at high concentrations effectively recapitulated the observations made in Figure 2E regarding infectivity using a co-delivery approach, it was hypothesized that limiting concurrent transfection by the cgRNA and ncgRNA liposomes would negatively impact vRNA infectivity. Therefore, to test the hypothesis that the enhancement of vRNA infectivity afforded by the ncgRNAs was dependent on the co-delivery of the two vRNA species into a given transfected cell, we diluted the mixed, independently formed vRNA-liposome complexes and evaluated their relative infectivity (Figure 3C). As demonstrated by the data in Figure 3D, the enhanced infectivity afforded by the presence of ncgRNA species was completely abrogated when the likelihood of co-delivery of both capped and noncapped into the same host cell was reduced by diluting their overall concentrations, negatively impacting the respective multiplicity of transfection.

While the above data indicates that the viral ncgRNAs enhance basal vRNA infectivity, they do not explicitly demonstrate that the noncapped RNAs are required to be viral in nature. Thus, before continuing to define the mechanism by which the viral ncgRNAs promote infectivity, assays designed to validate that the observed enhancements to vRNA infectivity were specifically dependent on the SINV viral-derived ncgRNAs were conducted. As described earlier for the co-delivery model, RNA-liposome complexes containing premixed ratios of capped and noncapped RNAs were generated and transfected into monolayers of permissive host cells. But, unlike before, the noncapped RNAs were not derived from SINV, and instead contained a Cypridina luciferase ORF (Figure 3E). Importantly, the presence of non-viral noncapped RNAs was unable to enhance vRNA infectivity, confirming that enhancement of vRNA infectivity is indeed dependent on the presence of virus-specific ncgRNAs (Figure 3F). To verify that the failure of the non-specific RNAs to enhance cgRNA

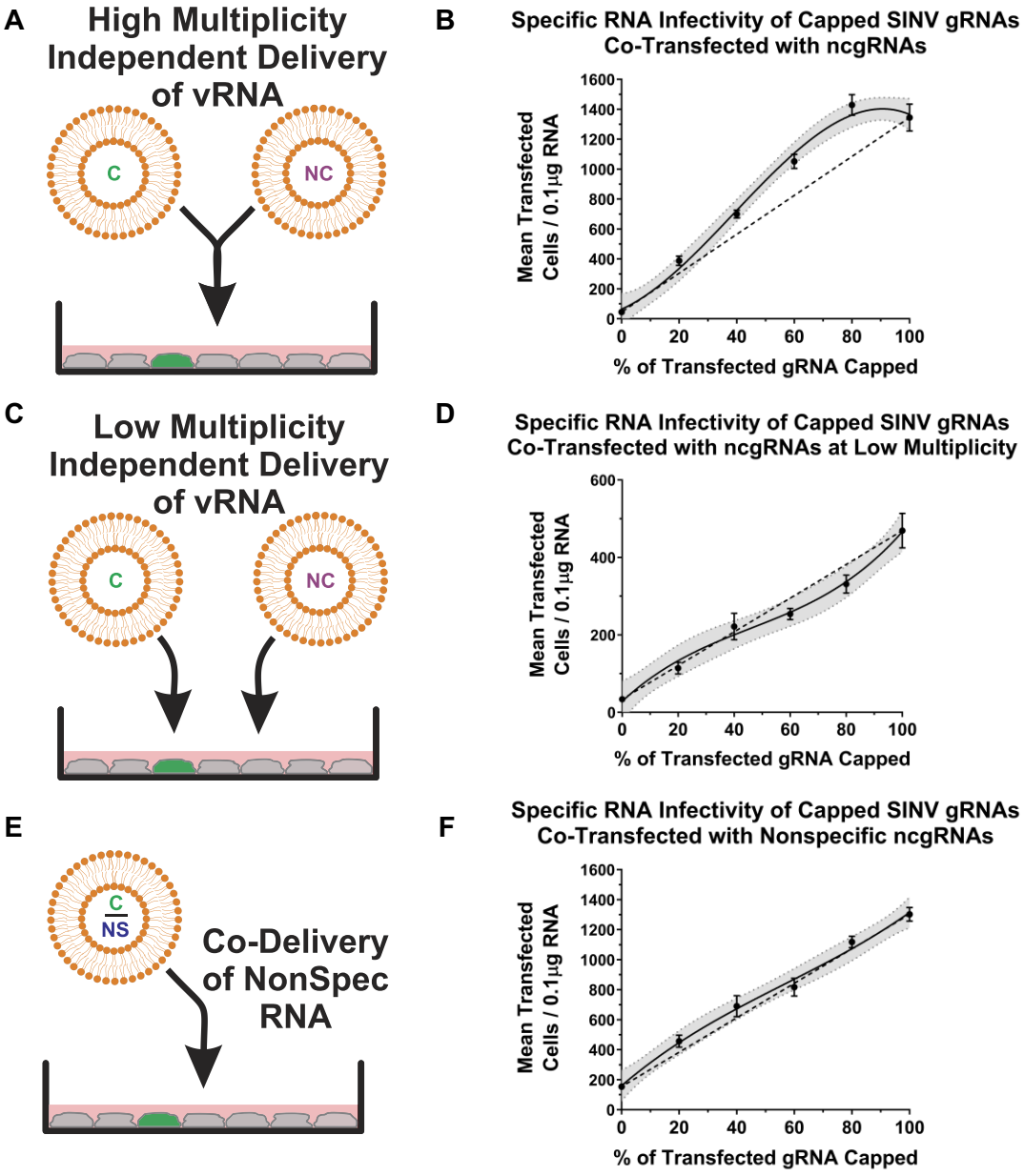

Figure 3. NcgRNA-mediated enhancement of RNA infectivity requires co-delivery of viral specific noncapped RNAs. (**A**) A schematic depicting the modified method of transfection used in panel (B), where liposomes containing solely cgRNAs or ncgRNAs were assembled and mixed at different ratios prior to delivery. (**B**) Quantitative analysis of relative vRNA specific infectivity following the independent delivery of cgRNAs and ncgRNAs at high multiplicity. (**C**) A schematic depicting the modified method of transfection used in panel (D), which are identical to those of panel (A) with the exception that the final mixture was diluted 1:4 after complex formation but prior to mixing before transfection. (**D**) Quantitative analysis of relative vRNA specific infectivity following the independent delivery of cgRNAs and ncgRNAs at low multiplicity. (**E**) A schematic depicting the modified method of transfection used in panel (F), where liposomes containing differing ratios of cgRNAs and a non-specific ncgRNAs were assembled prior to delivery. (**F**) Quantitative analysis of relative vRNA specific infectivity following co-delivery of cgRNAs and non-specific ncgRNAs. Data shown is the mean of six independent biological replicates, with the error bar representing the SD of the means. The solid line indicates the non-linear regression of the observed data, and the shaded area indicates the corresponding 95% confidence interval. The dashed line represents a linear model representing the purely cgRNA and ncgRNA populations.

infectivity was not due to the disparity in RNA length, these efforts were repeated with size-matched non-specific RNAs resulting in identical phenotypic observations, as shown in Supplemental Figure S4.

Taken together, these data confirm that the enhancement of vRNA infectivity afforded by ncgRNAs arises from a multi-hit kinetics involving the simultaneous delivery of the cgRNAs and ncgRNAs to the same host cell. More importantly, these data indicate that the noncapped RNAs must be virus-specific, as non-specific RNAs failed to enhance vRNA infectivity. The requirement for the ncgRNAs to be viral in origin is strongly suggestive of a sequence specificity of effect. Altogether, these observations suggest that a very early mechanism of action during replication is impacted by the co-delivery of the cgRNAs and ncgRNAs, leading the host cell past the point of no return for infection.

The ncgRNAs are not acting as a template for viral replication

Like all other positive-sense single-stranded RNA viruses, the gRNA of SINV must play at least two mutually exclusive and sequential activities during the viral replication. First, the gRNAs must serve as mRNA to express the viral proteins to yield functional replication complexes. At some point during this phase, the translating genomic vRNA has to switch its role from acting as a mRNA to acting as a template for the synthesis of complementary negative-strand RNA, from which new positive-strand RNAs are synthesized. The newly synthesized positive-sense vRNAs subsequently become available for further rounds of translation, replication or ultimately encapsidation to form progeny virus particles. The requirement of the incoming genomic vRNA to serve two distinct and incompatible functions during the early stages of viral infection where the concentration of gRNAs is limited represents a molecular bottleneck during the viral lifecycle. This is because the incoming genomic vRNA undergoing translation is occupied by multiple ribosomes, which in conjunction with the act of translation has been shown to inhibit vRNA replication by blocking the initiation of negative-sense vRNA synthesis (53,54). Although some host factors have been identified as interacting with SINV vRNAs at early times during infection, the mechanistic link between these host factors and the switch from translation to replication has not been discretely established (55).

The molecular bottleneck of having a single vRNA molecule that undergoes the dynamic process of altering its function from translation to replication could be readily alleviated by having two vRNA species that participate in the replication process via distinct and separate roles. As the cgRNAs and ncgRNAs fundamentally differ in their capacity to engage the host cap-dependent translational machinery, it was posited that the ncgRNAs are enhancing vRNA infectivity by playing a complementary role to the cgRNAs early during infection to alleviate the molecular bottleneck arising from a single-RNA system. In this model, the ncgRNAs, which are lacking translational capacity and free of ribosomes, are utilized by the viral RNA replicase complex as a template for vRNA synthesis early during infection when the incoming cgRNAs are simultaneously being translated by multiple ribosomes and indisposed to the replication machinery.

To test the two-RNA hypothesis of alphaviral vRNA replication, we measured cgRNA and ncgRNA replication activity/utilization by analyzing the expression of fluorescent reporter protein from newly synthesized genomic vRNAs arising from infection. Specifically, using a system derived from the co-delivery transfection model, the capped and noncapped vRNAs encode different fluorescent reporter proteins, such as mcherry and GFP, respectively. After 24 h of incubation, the fluorescence of individual reporter cells was measured as described for Figure 2 to identify the replicating RNA species, with the expectation that the preferentially replicating vRNA species will lead to increased expression of the corresponding fluorescent reporter via secondary translation of the newly synthesized gRNAs.

Contrary to expectations, and in direct refutation of the two-RNA replication hypothesis, the expression of the reporter protein encoded by the cgRNA species was dominant in the system, and that of the ncgRNA was rarely expressed and only observed in the complete absence of the cgRNA species (Figure 4A). This means that the RNA being synthesized and subsequently translated were almost exclusively made using the cgRNA as the parental template for minus strand synthesis. No double-labeled cells (as in those expressing both mCherry and GFP reporter fluorescence) were detected upon transfection of the mixed RNA species, even when the ratios of cgRNAs to ncgRNAs were competitive with one another. These results were readily reproduced when the fluorescent species was swapped between the cgRNA and ncgRNA species to ensure no artifactual limitations on the basis of the reporter gene (Supplemental Figure S3).

To determine whether the enhancement of infectivity afforded by the ncgRNAs contributed to the production of viral particles in addition to enhancing vRNA infectivity, viral titer quantitatively assessed using standard plaque assays enhanced by fluorescent detection prior. Consistent with data presented in Figure 4A, nearly all progeny viral plaques were derived from the cgRNA, as determined by the expression of the corresponding flourescent protein. To enable the true impact of the ncgRNAs on viral particle production on a per cell basis, and to cotnrol for maximum possible production per replicate, the assays were conducted in the presence and absence of NH_4Cl. As shown in Figure 4B, with the exception of the 0% cgRNA condition, all mixtures produced roughly equivalent numbers of viral particles, even when secondary rounds of viral infection in the assay plate were prevented via the addition of the lysosomotropic salt. Importantly, as per the data presented in Figure 2, the number of viral particles released per infected cell is increased in the presence of the ncgRNAs. Hence, from these data, it may be concluded that in the presence of ncgRNAs there is increased production of infectious viruses indicating an overall acceleration of virus RNA replication.

In summary, despite the novelty of the two-RNA hypothesis, the data above effectively conclude that the ncgRNAs do not act as a template to enhance replication. Nevertheless, the presence of ncgRNAs positively impacted the production of infectious virus particles through an unestablished means during the early stages of viral replication.

The ncgRNAs promote enhanced viral RNA synthesis/accumulation

The data presented above in Figure 4B and C implies that ncgRNAs are involved in accelerating viral replication because, despite an initial deficiency of translationally capable replicative vRNAs, highly similar end titers were observed. Given the necessity of co-delivery of the two RNA species into the same host cell for this effect, attention was focused on further defining the underlying viral biology to better understand the impact of the ncgRNAs to infection.

Firstly, to determine whether the enhanced/equivalent production of infectious virus was a result of increased vRNA transcription and replication, we quantified the genomic, subgenomic, and negative strand vRNAs at 2-, 4- and 8-hpt using strand-specific qRT-PCR. As shown in Figure 5 and similar to the observations made for infectious virus titers, the accumulations of the individual vRNA species were more or less biologically equivalent between all premixed ratios of gRNA and ncgRNA species and purely cgRNAs at indicated time points (despite being determined to be statistically different due to robust quantitative measurements). At early times af-

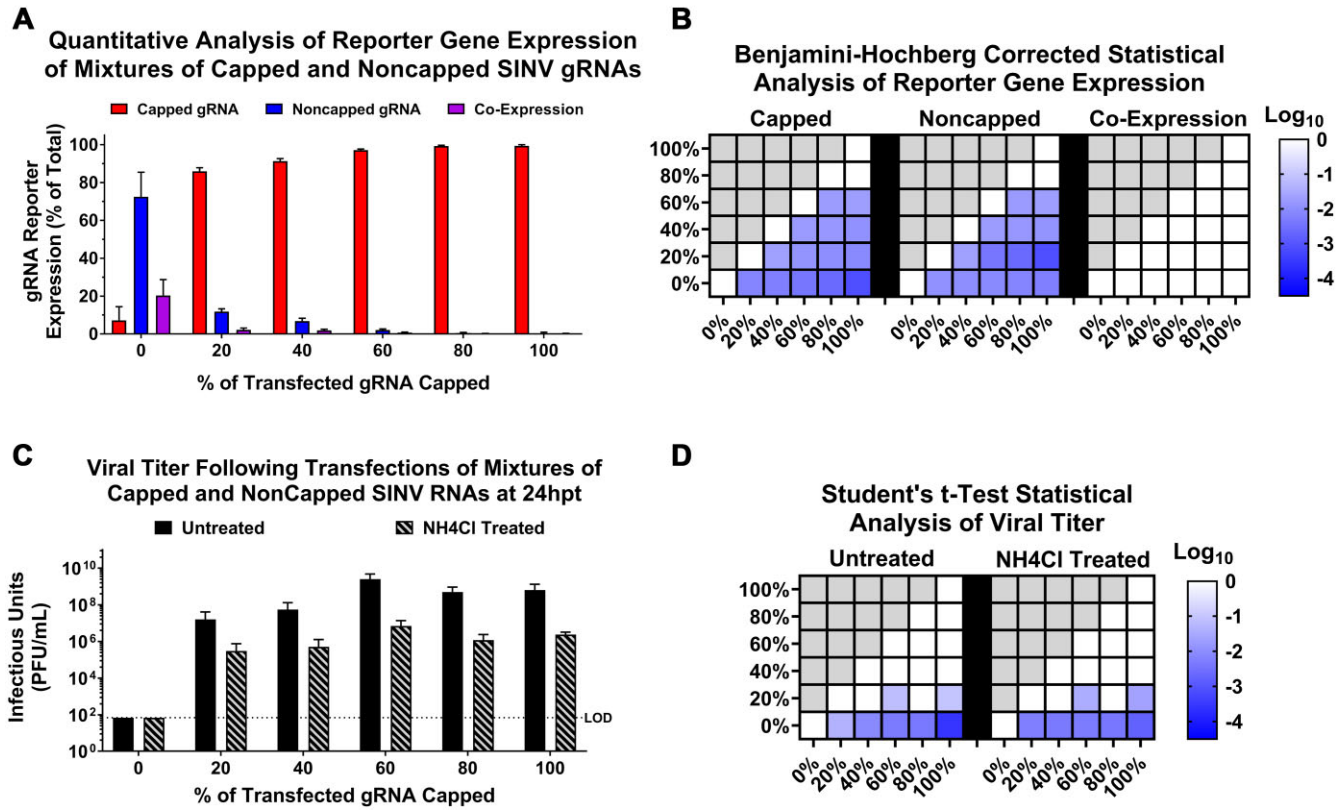

Figure 4. SINV cgRNAs are preferentially selected as the replication template during replication. (**A**) Mixtures of cgRNAs and ncgRNAs encoding different fluorescent reporter proteins were co-delivered via liposome transfection. At 24 hpt, using fluorescent microscopy, the infected cells were quantitatively assessed to determine the numbers of GFP, RFP and G&RFP reporter-positive cells. The quantitative data shown is the mean of six independent biological replicates, with the error bar representing the SD of the means. This data is further representative of another six independent biological replicates where the GFP and RFP-encoding nature of the cgRNAs and ncgRNAs were swapped. (**B**) The Benjamini–Hochberg corrected *P*-values for each of the possible comparisons. (**C**) Viral titers obtained using identical conditions of those for panel (A), with the exception that the transfected cells were either treated with ammonium chloride, or not, as indicated in the panel legend. (**D**) Student's *t*-test *P*-values for each of the possible comparisons across either the Untreated or the NH4Cl treated titer data sets.The quantitative data shown is the mean of three independent biological replicates, with the error bar representing the SD of the means.

ter transfection, the synthesis and accumulation of all three vRNA species remained similar, regardless of the cgRNAs and ncgRNAs delivered onto the cells. However, a marked increase in the level of individual vRNAs was observed at 8 h post-infection. There was no significant increase in genomic vRNA levels over the times assayed with the transfection condition corresponding to 0% capped, or purely ncgRNAs, indicating that these ncgRNAs are incapable of initiating meaningful replication.

Overall, these data demonstrate that the ncgRNAs contribute to vRNA infectivity and correlate positively with enhanced rates of viral RNA synthesis/accumulation. As a consequence, equivalent viral titers are observed between transfection conditions despite increased proportions of ncgRNAs incapable of driving viral replication by themselves. While these data provide further information regarding the biological impacts of the ncgRNAs, they are not directly informative as to precisely how viral infection is impacted at the molecular level necessitating further investigations.

The ncgRNAs contribute to enhance viral cgRNA translation

The data presented above indicates that accompanying ncgRNAs alongside cgRNAs confers a biological advantage to infectious potential and infectious virus particle production as the result of enhanced vRNA transcription and replication early in infection. As vRNA replication and translation are interconnected, since RNA replication is dependent on the production of the replicase complex via non-structural protein expression (25–27), viral gene expression during infection was quantitatively assessed. To determine whether increased translational activity was present and thereby supporting enhanced vRNA synthesis and accumulation, a SINV strain carrying nanoluciferase within the nsP3 gene, which allows for quantification of non-structural protein gene expression, was used. To assess translational activity, the co-delivery approach, as described above, was used to measured nanoluciferase activity at various time points.

As demonstrated by Figure 6, the level of nanoluciferase expression for the purely cgRNA population was significantly higher compared to the purely ncgRNA population at all evaluated time points, which was expected based on the basal translational capacity of the vRNA species. At 1- and 2-hpt, the cells transfected with mixed populations of cgRNAs and ncgRNAs demonstrated a trend of a roughly linear increase in nanoluciferase expression correlating with the increasing proportion of cgRNAs. However, at 4 hpt, the populations with mixed cgRNA and ncgRNA proportions attained translational activity akin to the level of purely cgRNAs. Similarly,

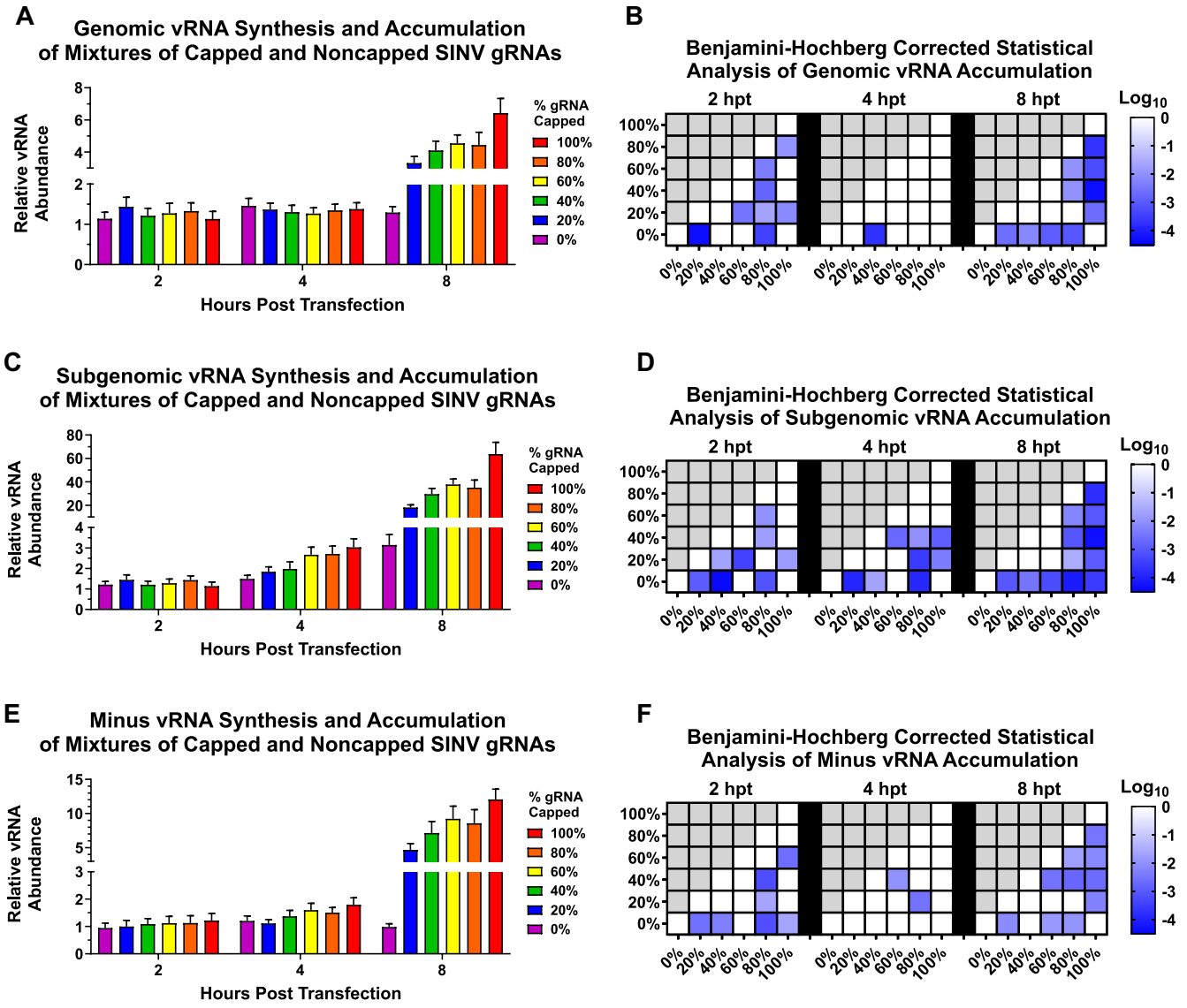

Figure 5. Viral RNA synthesis and accumulation is comparable across a wide range of cgRNA and ncgRNA conditions. (**A**), (**C**) and (**E**) depict the quantitative assessment of SINV vRNA synthesis following target specific qRT-PCR detection of the genomic, subgenomic and minus strand vRNAs with respect to time. For each vRNA species the data shown is relative to 0% capped at 2 hpt. The quantitative data shown is the mean of three independent biological replicates, with the error bar representing the SD of the means. (**B**), (**D**) and (**F**) represent the Benjamini–Hochberg corrected *P*-values for each of the possible comparisons within the individual time points assessed.

at 8 hpt, despite having a reduced level of translatable cgRNAs co-delivered to the host cell, mixtures containing predominantly ncgRNAs exhibited translational activity highly similar to the level of those with higher proportions of cgRNAs.

Altogether these data indicate that the co-delivery of mixtures containing predominately ncgRNAs exhibited rates of translational activity similarly to those with a higher proportion of cgRNAs. Furthermore, this demonstrates that the ncgRNAs are involved in promoting early events of viral replication, most likely gRNA translation, ultimately leading to productive infection and infectious virus release. Nonetheless, whether the enhanced gene expression seen is due to increased vRNA replication rates, enhanced translational activity of the accompanying cgRNAs, or through a confounding direct effect of ncgRNAs is unknown.

The ncgRNAs directly enhance early viral RNA translation

Here, the data presented above demonstrates that, using nanoluciferase-expressing vRNAs in a replication competent system, the translational activity of the cgRNAs is enhanced when accompanied by the ncgRNAs. Yet the true nature of this observation is still unclear, as the observed enhanced gene expression could be due to a ncgRNA-associated effect on the translation of initial incoming cgRNAs for viral protein synthesis, or enhanced vRNA replication resulting in the synthesis of additional new positive-sense vRNAs that are subsequently translatable.

To distinguish whether the effect is directly on cgRNA translation or indirect via vRNA replication followed by secondary translation of nascent cgRNAs, the above viral gene expression studies were repeated using a polymerase-defective

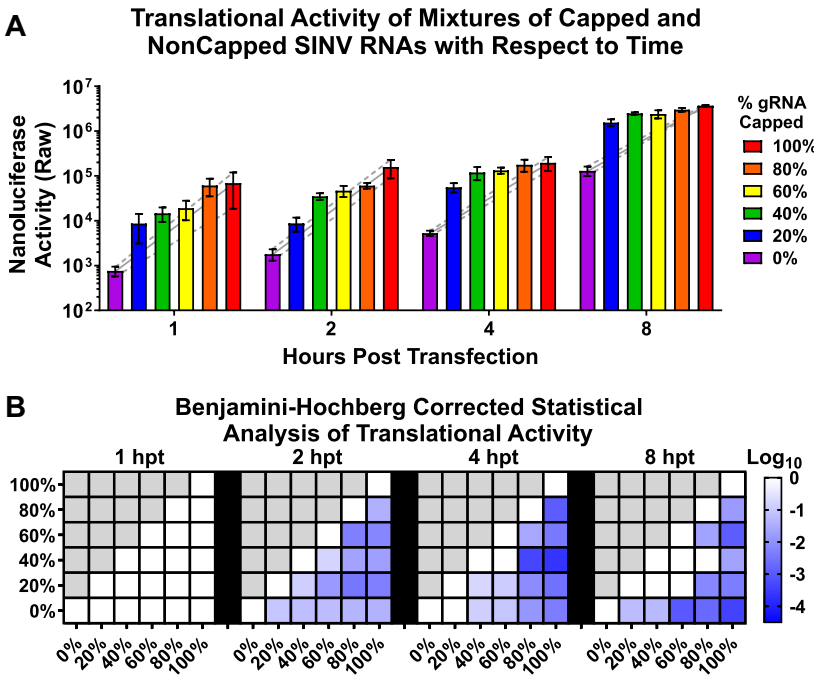

Figure 6. Viral non-structural protein gene expression is largely equivalent across a wide range of cgRNA and ncgRNA conditions. (**A**) Quantitative analysis of nanoluciferase expression encoded by replication competent gRNAs with respect to time. The quantitative data shown is the mean of three independent biological replicates, with the error bar representing the SD of the means. The solid and dashed lines show a linear model representing the purely cgRNA and ncgRNA populations. (**B**) The Benjamini–Hochberg corrected *P*-values for each of the possible comparisons within the individual time points assessed.

vRNA with the GDD motif within the RNA-dependent RNA polymerase (RdRp) nsP4 gene replaced by GAA, thereby inactivating the catalytic core. The mutation of the catalytic triad renders the RdRp activity null, precluding the synthesis of negative strands and the subsequent synthesis of translatable positive-sense vRNAs (56,57). Therefore, any nanoluciferase activity observed would be directly attributed to the translation of the vRNAs delivered into the cells by liposomes. Following the use of the co-delivery approach, nanoluciferase activities were measured immediately after transfection over 2.5-min intervals for up to 90 min in live-cell conditions.

As expected, the kinetics of luciferase activity increased with time, except for populations consisting of purely ncgRNAs which exhibited limited nanoluciferase activity. In all cases, the nanoluciferase signal was produced rapidly within 10 min of transfection, followed by an exponential phase lasting for ∼30–40 min. Interestingly, after the logarithmic phase the signal plateaued and remained largely stable. The overall levels of nanoluciferase activity and the rate at which the activities increased logarithmically indicated increased translational activity on a per gRNA basis for mixtures containing ncgRNAs (Figure 7A). Specifically, a notable observation was that the nanoluciferase activity of the 80% cgRNA mixture was almost identical to that of purely cgRNA populations despite having less translationally active vRNAs present.

Next, to dissect the direct effect of the ncgRNAs on the rate of early translation, the period corresponding to the exponential growth phase was examined in more detail by way of using non-linear regression analyses. To establish expected rates of early cgRNA translation for the mixed populations, as per the different amounts of translationally competent vRNAs, the observed rate (as per slope) for the pure cgRNA population was adjusted based on relative cgRNA content and the accumulation of nanoluciferase activity was forecasted. Thus, based on this model, a 20% reduction in nanoluciferase activity would be expected for a 20% reduction in cgRNAs, and so on. Comparative analysis of the observed translational rates (solid line) to the modeled rates (dashed line) indicates enhanced cgRNA translational activity across all ncgRNA containing conditions (Figure 7B). Note that the exponential growth curves corresponding to 100% cgRNAs is not shown, as these data were used to generate the expected model data and the observed and expected data would be identical. Thus, increased luciferase activity was observed for different ratios of mixed populations including purely ncgRNAs.

The quantification of cumulative observed to expected nanoluciferase activity, as determined by the AUC analysis for the exponential growth phase, revealed a statistically significant difference between modeled and observed nanoluciferase activities for all mixed population ratios (Figure 7C). Despite having no intrinsic translational capacity due to being noncapped, the pure ncgRNA population outperformed expectations as well when the non-linear model was adjusted to reflect the ncgRNA translational potential (as determined by the relative percent activity of the ncgRNA species relative to the cgRNA species).

Collectively, these data support the conclusion that the ncgRNAs have a direct influence on the translational capacity of the cgRNAs, and that enhancing the translational function of cgRNAs produces a cascading effect increasing vRNA replication and infectivity. On the whole, these data provide strong evidence that ncgRNAs are creating a pro-translational microenvironment for initial incoming cgRNAs.

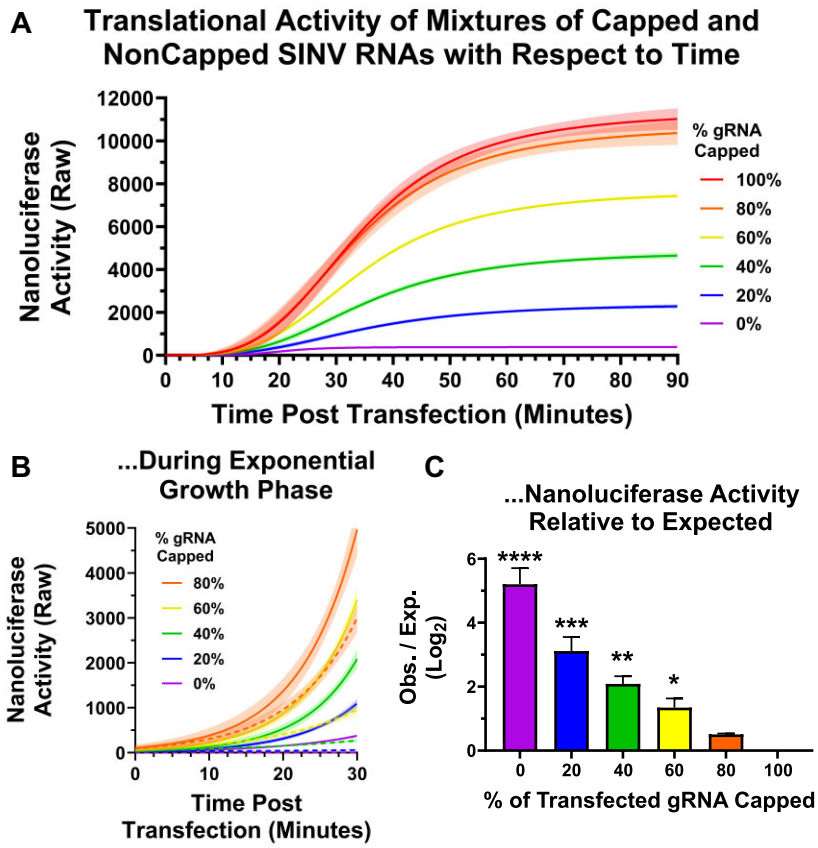

Figure 7. CgRNA translational activity is enhanced by the presence of ncgRNAs. (**A**) Real-time quantitative analysis of nanoluciferase expression from mixtures of replication incompetent cgRNAs and ncgRNAs with respect to time. The solid line indicates the non-linear regression of the observed data, and the shaded area indicates the corresponding 95% confidence interval. (**B**) Identical to panel (A); however, the window of observation and non-linear regression is cropped to the region where exponential signal growth was observed. Additionally, the corresponding color-coded dashed lines and shaded areas represent the expected data following the adjustment of the rate of translation observed for the 100% cgRNA conditions relative to the quantity of cgRNAs present in the system. (**C**) The cumulative ratio of Observed to Expected as determined by AUC analysis for the exponential growth phase. All quantitative data shown is the mean of six independent biological replicates, with the error bar representing the SD of the means. Statistical significance, as indicated by *, **, *** and ****, represent *P*-values of <0.05, <0.01, <0.001 and <0.0001 as determined by one-tailed Student's *t*-test, respectively.

Enhanced functionalization/translation of the cgRNAs requires translationally inactive ncgRNAs

As the vRNA species are identical sans the 5′ Type-0 cap structure, the basal capacity to engage in translation is the primary functional difference between the cgRNAs and ncgRNAs. The data so far indicate that the ncgRNAs influence early SINV life-cycle events, promoting overall vRNA infectivity through the enhancement of cgRNA translation. Given the inability of the ncgRNAs to undergo translation, it was next assessed whether changing the molecular function of the ncgRNAs (i.e. making them translationally competent via a cap-independent mechanism) impacts the observed phenomena. Firstly, to determine the impact on the capacity of the ncgRNAs to enhance the translation of incoming cgRNA, a similar nanoluciferase assay as described earlier was performed, except here the vRNAs included a synthetic Internal Ribosomal Entry Site (IRES) element incorporated into the native 5′UTR, namely the PS4 element, which drives cap-independent translation, as diagrammed in Figure 8A (42).

As shown in Figure 8B, nanoluciferase activity increased over time relative to cgRNA content; however, unlike the data presented in Figure 7, the nanoluciferase expression of purely ncgRNAs containing the PS4 synthetic IRES element was significantly higher when compared to wild type ncgRNAs. As before, nanoluciferase activity followed a logically anticipated stepwise progression with respect to cgRNA content. In short, the vRNA population with 80% cgRNAs demonstrated an ∼20% reduction in nanoluciferase expression compared to purely cgRNAs. These data indicate that the ncgRNAs are translationally active; nevertheless, the overall translational activity imparted by the PS4 synthetic IRES element is significantly less than that imparted by the 5′ cap. Whether this is due to decreased polysome association or defective ribosomal shuttling after termination is unknown.

As before, to determine the full extent of the impact of the ncgRNAs on translatability, the expected translational activity of the mixtures during the logarithmic phase were modeled. Unlike the experimental conditions of Figure 7, where the ncgRNAs had no appreciable contribution to nanoluciferase activity, the non-linear models used to quantitatively assess translational activity in Figure 8 accounted for the contributions of the cgRNA and ncgRNA populations. As shown in Figure 8C, the rate of nanoluciferase expression for all mixed populations of capped and noncapped vRNAs were in congruence with the modeled expected levels, and no statistically significant difference was observed between the modeled and observed nanoluciferase activities for all mixed ratios as per AUC analysis (Figure 8D).

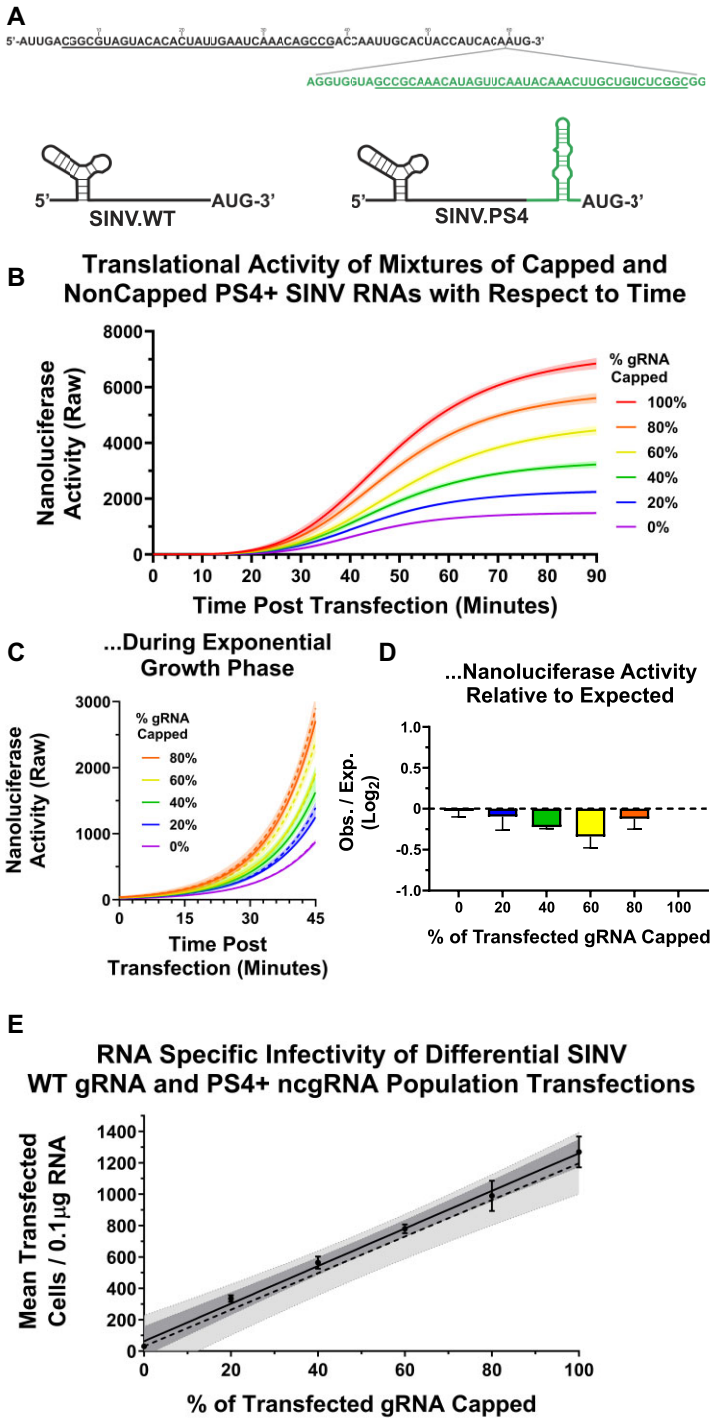

Figure 8. ncgRNA-mediated translational enhancement is abrogated after restoring the translational capacity of the ncgRNAs. (**A**) A schematic of the SINV PS4 + construct. The black nucleotide sequence represents the native SINV 5′UTR sequence, and the green nucleotide sequence called out by the diagonal lines represents the PS4 IRES element with the site of insertion indicated by gray lines. The underlined sequences represent known areas of secondary structure and the cartoon diagrams indicate the relative positioning of the structural elements. (**B**) Real-time quantitative analysis of nanoluciferase expression from mixtures of replication incompetent cgRNAs and synthetic IRES-element containing ncgRNAs with respect to time. The solid line indicates the non-linear regression of the observed data, and the shaded area indicates the corresponding 95% confidence interval. (**C**) Identical to panel B; however, the window of observation and non-linear regression is cropped to the region where exponential signal growth was observed. Additionally, the corresponding color-coded dashed lines and shaded areas represent the expected data following the adjustment of the rate of translation corresponding to the relative composition and contributions of the cgRNAs and ncgRNAs present in the system. (**D**) The cumulative ratio of Observed to Expected as determined by AUC analysis for the exponential growth phase. (**E**) Quantitative analysis of vRNA specific infectivity in the highly permissive BHK-21 cell line after transfection by liposomes containing mixtures of replication competent wild type cgRNA and PS4 + ncgRNAs encoding GFP and nanoluciferase, respectively. After incubation in the presence of ammonium chloride, viral infection was quantified via fluorescent reporter detection at 24 hpt. Data shown is the mean of six independent biological replicates, with the error bar representing the SD of the means. The solid line indicates the non-linear regression of the observed data, and the shaded area indicates the corresponding 95% confidence interval. The dashed line represents a linear model representing the purely cgRNA and ncgRNA populations.

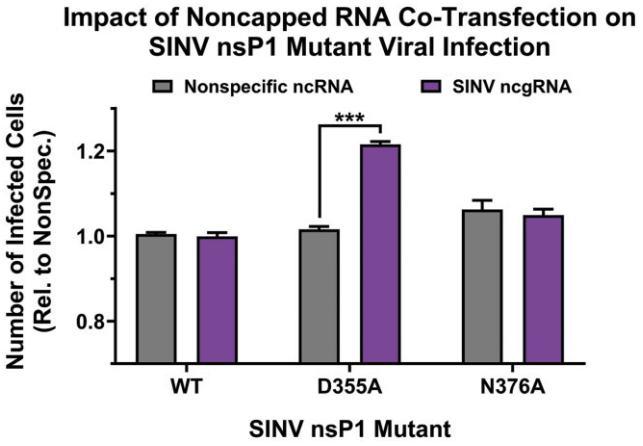

Figure 9. Co-transfection of ncgRNAs increases viral infectivity in particle populations with low ncgRNA content. BHK-21 cells were infected with either SINV.WT, SINV.D355A or SINV.N376A encoding a GFP reporter at MOEs of 300 or 30 while being concurrently infected with liposome complexes containing ncgRNAs encoding mCherry or the noncapped non-specific RNAs described earlier. After the adsorption/transfection period the media was removed and replaced with medium supplemented with ammonium chloride to block further entry. At 24 h post-treatment the cell monolayers were imaged and the number of reporter-positive cells was quantitified. The number of infectious events were internally normalized to the non-specific RNA control transfections for each virus. Data shown is the mean of six independent biological replicates (stemming from 3 at an MOE of 300, and 3 at an MOE of 30), and the error bar represents the SD of the means. Statistical significance, as indicated by *** relating to a *P*-value of <0.001, was determined by Student's *t*-test.

Finally, to better understand if translatability directly impacts the capacity of the ncgRNAs to enhance viral infection, vRNA infectivity was measured at 24 hpt using a co-delivery model of infection consisting of mixtures of replication competent wild type cgRNAs and ncgRNAs containing the PS4 synthetic IRES element. As shown in Figure 8E, the enhanced vRNA infectivity afforded by the ncgRNAs, as evident in Figure 2E, was abrogated during transfections of the corresponding ratios of cgRNAs and ncgRNAs where the translational capacity of the ncgRNAs had been restored.

These data indicate that the function of the ncgRNAs is dependent on their status as non-translating vRNAs, and thus have an independent but cooperative role during infection. Moreover, taken together, these data strongly suggest that vRNAs that are incapable of undergoing translation, specifically the ncgRNAs, are critically important to infectivity as they enhance the translational activity of the cgRNAs.

As the alphaviruses are positive-sense RNA viruses the viral gRNA represents the minimal infectious unit required to initiate infection. While cumulatively the data presented above support the conclusion that the ncgRNAs contribute to viral RNA infectivity via enhancing gRNA function, whether or not the ncgRNAs contribute to viral particle infectivity remained unknown.

To test the hypothesis that the ncgRNAs similarly contribute towards viral particle infectivity ncgRNAs were transfected during viral adsorption of SINV.WT, SINV.D355A, and SINV.N376A at MOEs of 300 and 30 particles per cell and the number of reporter gene-positive cells was quantified. To ensure that the impact of the ncgRNAs on viral infection was being quantified the viral particles and ncgRNAs encoded GFP and mCherry, respectively. As shown in Figure 9 the co-transfection of SINV ncgRNAs, but not non-specific noncapped RNAs, modestly enhanced the number of infected cells during SINV.D355A infections, but not during SINV.WT or SINV.N376A infections.

These data, despite being phenotypically mild, directly connect the presence of the ncgRNAs to enhanced viral particle infectivity during genuine viral infections. The magnitude of effect is likely negatively impacted by (i) a high likelihood of asynchronous entry between the liposome complexes and the viral particles, (ii) the requirement for co-delivery of the viral RNAs, and (iii) the potential for different entry pathways into the host cytoplasm. The absence of an effect during SINV.WT and SINV.N376A infections is straightforward to rationalize, as unlike the SINV.D355A mutant, these virus particle populations already have significant amounts of ncgRNA containing particle present in the milieu.

Discussion

The data presented above indicates that both the cgRNAs and ncgRNAs are required for successful alphaviral replication at the molecular level early during infection. To reach this conclusion, a series of compounding observations regarding the infectious potentials and impacts of the ncgRNAs set the stage for the observations made during this study. Briefly, using a sucrose gradient, it was determined that SINV particles produced from mammalian cell lines consisted of at least two distinct viral particle populations on the basis of particle density and these population exhibited different infectivity (43). Further characterization of the individual subpopulations revealed that a major feature correlating with infectivity was the presence of the 5′ cap structure, and that both cgRNAs and ncgRNAs were synthesized and packaged into viral particles (36). Recently, the observations from LaPointe *et al.* revealed a link between ncgRNA production and viral infectivity and pathogenesis via a reverse genetics approach (37,38). The alteration of the capping efficiency of the nsP1 protein associated with decreased ncgRNA production during infection resulting in reduced viral growth kinetics due, at least in part, to decreased viral particle production. Decreasing capping efficiency, as in favoring the production of the ncgRNAs, also negatively affected viral infection, presumably through the loss of vRNA functionalization as the number of viral particles produced was largely unaffected (38). While a reduction in gross particle production was observed following the enhancement of capping activity, the magnitude of effect was not wholly explained relative to the impact on viral titer. Thus, this observed discrepancy led to the hypothesis that the reduced production of the ncgRNAs impacts the infection potential of the virus particle population generated by the infected cells.

To address this research question, the infectivity of viral particles generated following infections of wild type SINV and nsP1 capping mutant viruses was quantified. These data showed that increasing or decreasing the capping efficiency of the SINV nsP1 protein negatively affects the infectivity of the viral particles. This reduction in infectivity correlated with inefficient replication thereby limiting the spread of plaques during the infectious center assays performed here. As alluded to earlier, the decreased particle infectivity observed while increasing the production of ncgRNAs as per the nsP1 N376A mutant is easy to reconcile as the ncgRNAs have low infectious potential, as directly confirmed by the data presented

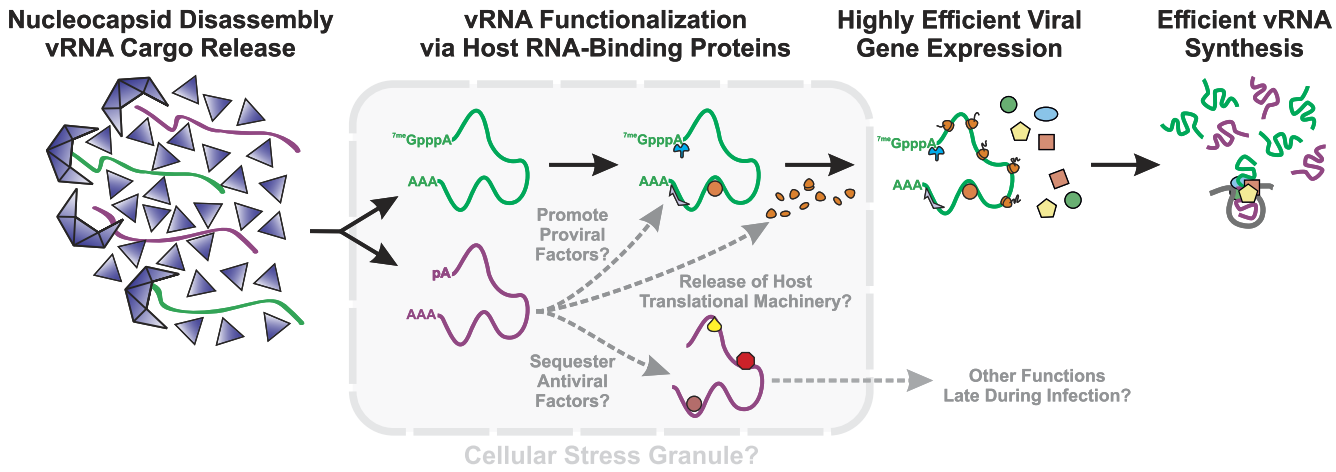

Figure 10. Proposed model of ncgRNA-mediated translational enhancement of cgRNAs. A diagram of the current working model regarding ncgRNA enhancement of alphaviral infection.

here in this study. Curiously, the decreased infectious capacity observed while increasing nsP1 capping efficiency, which in turn reduces the production of the ncgRNAs, was confounding, as the ncgRNAs themselves have been previously associated with noninfectious viral particles or particle populations with low specific infectivity (36). These data revealed a potential role for the ncgRNAs in the early stage of the viral lifecycle, establishing a need to understand the contribution of the individual gRNA species at the molecular level. Mechanistically, the data presented here supports the conclusion that the ncgRNAs support the translational activity of the cgRNAs during infection. Importantly, the capacity to enhance early viral gene expression was dependent on the ncgRNAs lacking translational activity, as modestly restoring the translational activity of the ncgRNAs via an IRES element abrogated cgRNA translational enhancement. Altogether, and as shown in Figure 10, the data presented here establish that the ncgRNAs contribute to the functionalization of the incoming cgRNA species, perhaps through one or more host/pathogen interactions via RNA:RNA or RNA:Protein interactions. Ongoing efforts to further characterize the precise molecular mechanisms and consequences of ncgRNAs to alphaviral replication are ongoing.

Specific infectivity is enhanced by multi-hit kinetics involving cgRNAs and ncgRNAs

Prior work has shown that vertebrate and invertebrate host cells produce heterogeneous populations of alphaviral particles (43). Consequently, the infection of the next host cell is a function of receiving multiple particles containing cgRNAs and ncgRNAs. While the specific contributions of the population components towards infection was, until now, largely unknown, the reality that subsequent infections were the result of exposures to the heterogeneous population remained true. To robustly test the contributions of each of the viral gRNA species to infection, the reductionist approach involving transfection of well-defined RNA mixtures applied in this study was utilized. The single-cell transfection assays involving the transfection of pre-mixed capped and noncapped SINV gRNA complexes showed that the vRNA infectivity is non-linear, and the presence of ncgRNAs enhances the infectivity of the mixed liposomes beyond the contribution of the individual components. This enhancement is supportive of a multi-hit kinetic phenomenon as both capped and noncapped vRNA species are required to be delivered into the same cell to enhance infectivity. Whether there is a specific order to which the ncgRNAs and cgRNAs must be introduced to the host cell for the enhancement effect to occur is unknown at this time. Nonetheless, the stochiometric ratios of ncgRNA and cgRNA containing viral particles suggests that having the ncgRNAs enter prior to, or at the very least simultaneously with, the cgRNAs is required for enhancement.

Nonetheless, it is important to correlate the findings of this study with others that measured the levels of ncgRNAs present in viral particle populations derived from genuine infections. Prior work has established that the cgRNA to ncgRNA ratios differ on the basis of the host species, alphavirus species, and the strain of virus being assessed. For the SINV strain used in the reductionist studies presented here, the native populations of viral particles correspond roughly to the 20:80 cgRNA to ncgRNA ratio. In the analyses reported here, the most efficient infection conditions (with ∼3-fold enhancement of early viral gene expression) was observed for the ratio of 20:80, which is consistent with wild type particles produced from vertebrate hosts (36). In the same vein, the corresponding ratios of cgRNA to ncgRNAs that were found for the nsP1 D355A mutant (with ∼4-fold higher cgRNAs compared to wild type) and the nsP1 N376A mutant (with ∼75% less cgRNA compared to wild type) were less efficient in promoting vRNA infectivity (37). The observation that wild type particle populations exhibit optimal ratios for RNA infectivity indicates that accompanying cgRNA with ncgRNA is advantageous for SINV infectivity and likely driven by selective processes.

If the ncgRNAs are not acting directly, what is their function?

The SINV genome consists of at least a 5′ capped single-stranded positive-sense RNA, which serves, as confirmed here, as a template for both translation and replication. The data shown here demonstrates the requirement of co-delivery of both vRNA species which led to the inference that alphaviruses, such as SINV, may have a more efficient way to replicate through a ‘two RNA’ co-delivery system benefitting the early stages of infection. The initial hypothesis regarding

a 'two RNA' system was the supposition that, as the ncgRNAs are genetically identical to cgRNAs with the only primary difference being the presence of a 5′ cap structure, they may function as a readily available template for the synthesis of the nascent vRNAs as all necessary *cis*-acting RNA replication elements are present (58–61). Using this 'two RNA' mechanism, SINV may overcome the delay in the replication caused by the switching of a single RNA species from serving as a mRNA to a template for minus strand synthesis, thereby minimizing the time required to produce mature viral particles. However, contrary to this hypothesis, it was observed that the ncgRNAs did not act as a template for the synthesis of the minus strand vRNAs, and that the cgRNAs were primarily associated with vRNA synthesis and replication. The precise cause of the transition of the incoming viral cgRNA from a mRNA to a template for vRNA synthesis is still unclear for the alphaviruses; however, the ncgRNAs serve no apparent direct role in this transition event. Nonetheless, an indirect role through the synthesis of viral proteins, or the co-optation of host factors, cannot be excluded.

Another finding of this study was the identification of the 5′ cap as a major determinant for minus-strand vRNA synthesis, providing further evidence that alphaviral replication complexes preferentially select replication templates in *cis* despite efficient replication in *trans* (62). Additionally, not only the presence of the 5′ and 3′ end of the genome but also the interaction between the 5′ and 3′ end of the genome is suggested to be essential for the effective initiation of minus strand synthesis (58–60). The interaction between the 5′ and 3′ end of the genome through the interaction of the host eIF4G component of eIF4F with Poly(A) Binding Protein (PABP) ultimately leading to circularization of the mRNA is a well-characterized feature of translation (63,64). This circularization of the mRNA, which greatly enhances translational activity, may also be important for the initiation of minus-strand vRNA synthesis by making the switch from translation to replication as suggested by Frolov *et al.* (2001) (58). This switch may be triggered due to the direct or indirect interaction of the 5′ cap structure with the viral replicase complex that brings it within proximity to the 3′ end of circularized RNA formed during translation. Thus, future studies should focus their investigation on understanding the interaction of host initiation factors with the viral replicase complex in SINV in the context of the 5′ cap as a potential determinant of activity.

The ncgRNAs act as a translational enhancer of the incoming cgRNAs to influence overall infection

The data presented here demonstrates enhanced vRNA translational activity and replication of the cgRNAs in the presence of ncgRNAs, which together sufficiently support infectivity and infectious virus production. In the presence of ncgRNAs, the incoming cgRNAs exhibited translational rate enhancements dependent on the overall ratios of the two RNA species. The enhanced translation of the replicase complex led to a cumulative effect regarding vRNA synthesis, where despite lower cgRNA amounts, mixtures containing ncgRNAs significantly outperformed expectations. However, the precise mechanism by which the ncgRNAs promote the translation of the cgRNA is yet to be fully elucidated.

The capacity for the translationally inactive ncgNAs to promote the translation of the cgRNAs is very puzzling. However, the bulk of the data lends several clues as to how this may be achieved, or at least a rough framework for how the ncgRNAs are acting. The enhancement of cgRNA translational activity is dependent on the ncgRNAs themselves not being able to be translated as evidenced by the loss of enhancement when translation of the ncgRNAs is driven by an artificial IRES element. Thus, the readthrough of the non-structural ORF appears to be detrimental to ncgRNA function, potentially indicating that *cis*- or *trans*-acting RNA interactions driven by sequences locally contained in the non-structural ORF are critical to ncgRNA function. A leading hypothesis regarding ncgRNA molecular function is that they serve to sequester antiviral host RNA-binding proteins, while also promoting the association of pro-translational factors to the cgRNAs. Therefore, the identification of and the mapping of the ncgRNAs and any interacting host proteins will be the next avenue to explore to better understand the mechanism of ncgRNA.

Translationally inactive host mRNAs are found in the cytoplasmic stress granules (SGs), where transcripts may be reactivated towards translation or slated for degradation. As the viral gRNAs are essentially nude of the host factors involved in replication, it is possible that they may be directed towards the SG as translationally inactive RNAs. As the SG is rich in translational machinery, including rRNAs, proteins of the small ribosomal subunits, translational initiation factors such as eIF3 and eIF4F and RNA-binding proteins known to functionalize host RNAs, SINV may be utilizing the ncgRNAs either to exploit the SGs for redistribution of translational machinery to the cgRNAs or to sequester host mRNA surveillance or antiviral factors. Although SGs are a known component of antiviral defense, it is suggested that viruses not only interfere with the assembly of SGs but also utilize the SG proteins for their replication (65,66). Two core components of SGs (i.e. TIA-1 and TIAR) which arrest translation, bind to translationally inactive mRNAs and sequester them into SGs. Perhaps these host factors are aggregated towards the ncgRNAs, preventing their association with the cgRNAs thereby enhancing translational efficiency. Studies have also reported binding of TIA-1 and TIAR to other positive-sense RNA viruses including West Nile virus and Tick-Borne Encephalitis virus (67,68).

Potential roles of the ncgRNAs in the invertebrate host

Previous studies have demonstrated that mammalian-derived alphaviruses manifest higher infectivity in mosquito cells, and vice versa, indicating that there are differences between virus particles derived from mosquito cells and mammalian cells (36,43,69). Production of both 'light' and 'heavy' particles, with the production of mostly light particles being associated with mammalian cells while production of only 'heavy' particles associated with mosquito cells, proved to be one of the observed differences (43). In mammalian cells, the 'light' particle species predominantly contained ncgRNAs, and were less infectious compared to highly infectious 'heavy' particles, which contained predominantly cgRNAs (36). A later assessment of tissues from Ross River virus infected mouse models indicated that only 'light' particles are present in mouse serum (69). Hence, following the infectious blood meal, a naïve mosquito would be inoculated with 'light' particles during feeding. The same study also concluded that 'light' particles showed greater efficiency in infecting midgut tissues compared to 'heavy' particles. Interestingly, the vertebrate-derived 'light' particles, which again predominately contain ncgRNAs,

facilitated the infection of mosquitoes, strongly suggesting the importance of the ncgRNAs in successful alphaviral transmission between the vertebrate host and the invertebrate vector. Collectively, this study provides the functional role of the ncgRNAs in initiating an enhanced infection through translation in the vertebrate host. Since, at this time, the characterization of the ncgRNAs in mosquito hosts has not been exhaustively performed, it may be speculated that the ncgRNAs, through similar mechanisms, may initiate a productive infection and dissemination of the virus in the mosquito host. Work is continuing to determine whether alphaviral ncgRNAs utilize similar mechanisms to promote infection of mosquito cells.

Other potential role(s) of the ncgRNAs during infection and limitations

The data presented here identifies a previously unknown role for the ncgRNAs in regard to the establishment of viral infection via increasing the RNA infectious potential. While the impact of the ncgRNAs on the likelihood that a 'go/no-go' threshold to replication is met resulting in productive infection is clear, it likely to be far from the only or final contribution of the ncgRNAs to infection. Indeed, as an example the production of the ncgRNAs has been previously implicated in regards to the production of viral particles. While the precise mechanism of this phenomenon remains unknown, a leading hypothesis is that the ncgRNAs support particle assembly by excluding host factors involved in the disassembly process. Unfortunately, a limitation of the studies presented here is that the experimental methodology is unable to address the role(s) of the ncgRNAs on particle assembly, specifically due to- i) the use of wild type nsP1 proteins in all reductionist systems testing the contributions of the ncgRNAs to infectivity, and ii) an inability to deliver ncgRNAs at stoichiometric amounts meaningful during late infection. As the wild type nsP1 protein background was used it can be effectively ruled out as the basis for the reported observations; however, the use of the wild type nsP1 precludes the ability to use these data to infer about later roles for the ncgRNAs as the intracellular environment will be invariably wild type. This limitation, while double-edged, was critically important to defining the contribution of the ncgRNAs to viral RNA and particle infectivity. Similarly, the possibility that the basal mutations of the nsP1 protein impact these biological phenomenon on a broader scale remains, and further characterization of the mutants beyond their impact on viral capping efficiency is warranted.

Data availability

All original data is presented in the context of the manuscript, and no large data sets requiring deposition were generated. The data underlying this article will be shared on reasonable request to the corresponding author.

Supplementary data

Supplementary Data are available at NAR Online.

Acknowledgements

We thank the members of the laboratories of KJ Sokoloski, D. Chung and R. Hardy, for their invaluable input during the development and execution of this project, and the preparation/editing of this manuscript.

Funding

National Institute of Allergy and Infectious Diseases [R01 AI153275 to K.J.S.]; National Institute of General Medical Sciences [P20 GM125504 to K.J.S.; R. Lamont]; Integrated Programs in Biomedical Sciences (to D.K. and C.M.I.); University of Louisville (to K.J.S.); University of Louisville School of Medicine. Funding for open access charge: University of Louisville.

Conflict of interest statement

None declared.

References

1. Knipe,D., Howley,P., Griffin,D., Lamb,R., Martin,M., Roizman,B. and Straus,S. (2013) *Fields Virology, Volumes 1 and 2*. Lippincott Williams & Wilkins: Philadelphia, PA, USA.
2. Strauss,J.H. and Strauss,E.G. (1994) The alphaviruses: gene expression, replication, and evolution. *Microbiol. Rev.*, **58**, 491–562.
3. Westcott,C.E., Isom,C.M., Karki,D. and Sokoloski,K.J. (2023) Dancing with the devil: a review of the importance of host RNA-binding proteins to alphaviral RNAs during infection. *Viruses*, **15**, 164.
4. Calisher,C.H. (1994) Medically important arboviruses of the United States and Canada. *Clin. Microbiol. Rev.*, **7**, 89–116.
5. Jose,J., Snyder,J.E. and Kuhn,R.J. (2009) A structural and functional perspective of alphavirus replication and assembly. *Future Microbiol*, **4**, 837–856.
6. Young,A.R., Locke,M.C., Cook,L.E., Hiller,B.E., Zhang,R., Hedberg,M.L., Monte,K.J., Veis,D.J., Diamond,M.S. and Lenschow,D.J. (2019) Dermal and muscle fibroblasts and skeletal myofibers survive chikungunya virus infection and harbor persistent RNA. *PLoS Pathog.*, **15**, e1007993.
7. Forrester,N.L., Wertheim,J.O., Dugan,V.G., Auguste,A.J., Lin,D., Adams,A.P., Chen,R., Gorchakov,R., Leal,G., Estrada-Franco,J.G., *et al.* (2017) Evolution and spread of Venezuelan equine encephalitis complex alphavirus in the Americas. *PLoS Negl. Trop. Dis.*, **11**, e0005693.
8. Ronca,S.E., Dineley,K.T. and Paessler,S. (2016) Neurological sequelae resulting from encephalitic alphavirus infection. *Front. Microbiol.*, **7**, 959.
9. Weaver,S.C., Salas,R., Rico-Hesse,R., Ludwig,G.V., Oberste,M.S., Boshell,J. and Tesh,R.B. (1996) Re-emergence of epidemic Venezuelan equine encephalomyelitis in South America. VEE Study Group. *Lancet*, **348**, 436–440.
10. Zacks,M.A. and Paessler,S. (2010) Encephalitic alphaviruses. *Vet. Microbiol.*, **140**, 281–286.
11. Burt,F.J., Chen,W., Miner,J.J., Lenschow,D.J., Merits,A., Schnettler,E., Kohl,A., Rudd,P.A., Taylor,A., Herrero,L.J., *et al.* (2017) Chikungunya virus: an update on the biology and pathogenesis of this emerging pathogen. *Lancet Infect. Dis.*, **17**, e107–e117.
12. Brummer-Korvenkontio,M., Vapalahti,O., Kuusisto,P., Saikku,P., Manni,T., Koskela,P., Nygren,T., Brummer-Korvenkontio,H. and Vaheri,A. (2002) Epidemiology of Sindbis virus infections in Finland 1981-96: possible factors explaining a peculiar disease pattern. *Epidemiol. Infect.*, **129**, 335–345.
13. Kurkela,S., Manni,T., Myllynen,J., Vaheri,A. and Vapalahti,O. (2005) Clinical and laboratory manifestations of Sindbis virus infection: prospective study, Finland, 2002-2003. *J. Infect. Dis.*, **191**, 1820–1829.

14. Laine,M., Luukkainen,R., Jalava,J., Ilonen,J., Kuusistö,P. and Toivanen,A. (2000) Prolonged arthritis associated with Sindbis-related (Pogosta) virus infection. *Rheumatology (Oxford)*, **39**, 1272–1274.
15. Adouchief,S., Smura,T., Sane,J., Vapalahti,O. and Kurkela,S. (2016) Sindbis virus as a human pathogen-epidemiology, clinical picture and pathogenesis. *Rev. Med. Virol.*, **26**, 221–241.
16. Suvanto,M.T., Uusitalo,R., Otte Im Kampe,E., Vuorinen,T., Kurkela,S., Vapalahti,O., Dub,T., Huhtamo,E. and Korhonen,E.M. (2022) Sindbis virus outbreak and evidence for geographical expansion in Finland, 2021. *Euro Surveill.*, **27**, 2200580.
17. Campbell,L.P., Luther,C., Moo-Llanes,D., Ramsey,J.M., Danis-Lozano,R. and Peterson,A.T. (2015) Climate change influences on global distributions of dengue and chikungunya virus vectors. *Phil. Trans. R. Soc. Lond. B Biol. Sci.*, **370**, 20140135.
18. Weaver,S.C. (2013) Urbanization and geographic expansion of zoonotic arboviral diseases: mechanisms and potential strategies for prevention. *Trends Microbiol.*, **21**, 360–363.
19. Kendrick,K., Stanek,D. and Blackmore,C. (2014) Notes from the field: transmission of chikungunya virus in the continental United States–Florida, 2014. *MMWR Morb. Mortal. Wkly. Rep.*, **63**, 1137.
20. Weaver,S.C. (2014) Arrival of chikungunya virus in the new world: prospects for spread and impact on public health. *PLoS Negl Trop Dis*, **8**, e2921.
21. Slifka,D.K., Raué,H.P., Weber,W.C., Andoh,T.F., Kreklywich,C.N., DeFilippis,V.R., Streblow,D.N., Slifka,M.K. and Amanna,I.J. (2022) Development of a next-generation chikungunya virus vaccine based on the HydroVax platform. *PLoS Pathog.*, **18**, e1010695.
22. Strauss,E.G., Rice,C.M. and Strauss,J.H. (1984) Complete nucleotide sequence of the genomic RNA of Sindbis virus. *Virology*, **133**, 92–110.
23. Hefti,E., Bishop,D.H., Dubin,D.T. and Stollar,V. (1975) 5' nucleotide sequence of Sindbis viral RNA. *J. Virol.*, **17**, 149–159.
24. Griffin,D.E. (2002) Alphaviruses. In: *Wiley Encyclopedia of Molecular Medicine*. https://doi.org/10.1002/0471203076.emm0776.
25. Lemm,J.A., Rümenapf,T., Strauss,E.G., Strauss,J.H. and Rice,C.M. (1994) Polypeptide requirements for assembly of functional Sindbis virus replication complexes: a model for the temporal regulation of minus- and plus-strand RNA synthesis. *EMBO J.*, **13**, 2925–2934.
26. Shirako,Y. and Strauss,J.H. (1994) Regulation of Sindbis virus RNA replication: uncleaved P123 and nsP4 function in minus-strand RNA synthesis, whereas cleaved products from P123 are required for efficient plus-strand RNA synthesis. *J. Virol.*, **68**, 1874–1885.
27. Rupp,J.C., Sokoloski,K.J., Gebhart,N.N. and Hardy,R.W. (2015) Alphavirus RNA synthesis and non-structural protein functions. *J. Gen. Virol.*, **96**, 2483–2500.
28. Shirako,Y. and Strauss,J.H. (1990) Cleavage between nsP1 and nsP2 initiates the processing pathway of Sindbis virus nonstructural polyprotein P123. *Virology*, **177**, 54–64.
29. Owen,K.E. and Kuhn,R.J. (1996) Identification of a region in the Sindbis virus nucleocapsid protein that is involved in specificity of RNA encapsidation. *J. Virol.*, **70**, 2757–2763.
30. Weiss,B., Nitschko,H., Ghattas,I., Wright,R. and Schlesinger,S. (1989) Evidence for specificity in the encapsidation of Sindbis virus RNAs. *J. Virol.*, **63**, 5310–5318.
31. Melancon,P. and Garoff,H. (1987) Processing of the Semliki Forest virus structural polyprotein: role of the capsid protease. *J. Virol.*, **61**, 1301–1309.
32. Ahola,T. and Kääriäinen,L. (1995) Reaction in alphavirus mRNA capping: formation of a covalent complex of nonstructural protein nsP1 with 7-methyl-GMP. *Proc. Natl Acad. Sci. U.S.A.*, **92**, 507–511.
33. Ahola,T., Laakkonen,P., Vihinen,H. and Kääriäinen,L. (1997) Critical residues of Semliki Forest virus RNA capping enzyme involved in methyltransferase and guanylyltransferase-like activities. *J. Virol.*, **71**, 392–397.
34. Law,Y.-S., Utt,A., Tan,Y.B., Zheng,J., Wang,S., Chen,M.W., Griffin,P.R., Merits,A. and Luo,D. (2019) Structural insights into RNA recognition by the Chikungunya virus nsP2 helicase. *Proc. Natl Acad. Sci. U.S.A.*, **116**, 9558–9567.
35. Vasiljeva,L., Merits,A., Auvinen,P. and Kääriäinen,L. (2000) Identification of a novel function of the alphaviruscapping apparatus: RNA 5′-triphosphatase activity of Nsp2. *J. Biol. Chem.*, **275**, 17281–17287.
36. Sokoloski,K.J., Haist,K.C., Morrison,T.E., Mukhopadhyay,S. and Hardy,R.W. (2015) Noncapped alphavirus genomic RNAs and their role during infection. *J. Virol.*, **89**, 6080–6092.
37. LaPointe,A.T., Landers,V.D., Westcott,C.E. and Sokoloski,K.J. (2020) Production of noncapped genomic RNAs is critical to Sindbis virus disease and pathogenicity. *mBio*, **11**, e02675-20.
38. LaPointe,A.T., Moreno-Contreras,J. and Sokoloski,K.J. (2018) Increasing the capping efficiency of the Sindbis Virus nsP1 protein negatively affects viral infection. *mBio*, **9**, e02342-18.
39. Sokoloski,K.J., Hayes,C.A., Dunn,M.P., Balke,J.L., Hardy,R.W. and Mukhopadhyay,S. (2012) Sindbis virus infectivity improves during the course of infection in both mammalian and mosquito cells. *Virus Res.*, **167**, 26–33.
40. Sokoloski,K.J., Nease,L.M., May,N.A., Gebhart,N.N., Jones,C.E., Morrison,T.E. and Hardy,R.W. (2017) Identification of interactions between Sindbis virus capsid protein and cytoplasmic vRNA as novel virulence determinants. *PLoS Pathog.*, **13**, e1006473.
41. Frolova,E., Gorchakov,R., Garmashova,N., Atasheva,S., Vergara,L.A. and Frolov,I. (2006) Formation of nsP3-specific protein complexes during Sindbis virus replication. *J. Virol.*, **80**, 4122–4134.
42. Venkatesan,A. and Dasgupta,A. (2001) Novel fluorescence-based screen to identify small synthetic internal ribosome entry site elements. *Mol. Cell. Biol.*, **21**, 2826–2837.
43. Sokoloski,K.J., Snyder,A.J., Liu,N.H., Hayes,C.A., Mukhopadhyay,S. and Hardy,R.W. (2013) Encapsidation of host-derived factors correlates with enhanced infectivity of Sindbis virus. *J. Virol.*, **87**, 12216–12226.
44. Landers,V.D., Thomas,M., Isom,C.M., Karki,D. and Sokoloski,K.J. (2024) Capsid protein mediated evasion of IRAK1-dependent signalling is essential to Sindbis virus neuroinvasion and virulence in mice. *Emerg Microbes Infect*, **13**, 2300452.
45. Igloi,G.L. and Kössel,H. (1987) [27]Use of boronate-containing gels for electrophoretic analysis of both ends of RNA molecules. *Methods in Enzymology*. Academic Press, Amsterdam, The Netherlands, Vol. **155**, pp. 433–448.
46. Luciano,D.J. and Belasco,J.G. (2019) Analysis of RNA 5' ends: phosphate enumeration and cap characterization. *Methods*, **155**, 3–9.
47. Beverly,M., Dell,A., Parmar,P. and Houghton,L. (2016) Label-free analysis of mRNA capping efficiency using RNase H probes and LC-MS. *Anal. Bioanal.Chem.*, **408**, 5021–5030.
48. Fuchs,A.L., Neu,A. and Sprangers,R. (2016) A general method for rapid and cost-efficient large-scale production of 5' capped RNA. *RNA*, **22**, 1454–1466.
49. Nwokeoji,A.O., Chou,T. and Nwokeoji,E.A. (2023) Low resource integrated platform for production and analysis of capped mRNA. *ACS Synth. Biol.*, **12**, 329–339.
50. Santoro,S.W. and Joyce,G.F. (1997) A general purpose RNA-cleaving DNA enzyme. *Proc. Natl Acad. Sci. U.S.A.*, **94**, 4262–4266.
51. Moradian,H., Lendlein,A. and Gossen,M. (2020) Strategies for simultaneous and successive delivery of RNA. *J. Mol. Med. (Berl.)*, **98**, 1767–1779.
52. Zhang,H., Bussmann,J., Huhnke,F.H., Devoldere,J., Minnaert,A.K., Jiskoot,W., Serwane,F., Spatz,J., Röding,M., De Smedt,S.C., *et al.* (2022) Together is better: mRNA co-encapsulation in lipoplexes is

required to obtain ratiometric co-delivery and protein expression on the single cell level. *Adv. Sci. (Weinh.)*, **9**, e2102072.
53. Barton,D.J., Morasco,B.J. and Flanegan,J.B. (1999) Translating ribosomes inhibit poliovirus negative-strand RNA synthesis. *J. Virol.*, **73**, 10104–10112.
54. Gamarnik,A.V. and Andino,R. (1998) Switch from translation to RNA replication in a positive-stranded RNA virus. *Genes Dev.*, **12**, 2293–2304.
55. Cristea,I.M., Rozjabek,H., Molloy,K.R., Karki,S., White,L.L., Rice,C.M., Rout,M.P., Chait,B.T. and MacDonald,M.R. (2010) Host factors associated with the Sindbis virus RNA-dependent RNA polymerase: role for G3BP1 and G3BP2 in virus replication. *J. Virol.*, **84**, 6720–6732.
56. Rubach,J.K., Wasik,B.R., Rupp,J.C., Kuhn,R.J., Hardy,R.W. and Smith,J.L. (2009) Characterization of purified Sindbis virus nsP4 RNA-dependent RNA polymerase activity in vitro. *Virology*, **384**, 201–208.
57. Tomar,S., Hardy,R.W., Smith,J.L. and Kuhn,R.J. (2006) Catalytic core of alphavirus nonstructural protein nsP4 possesses terminal adenylyltransferase activity. *J. Virol.*, **80**, 9962–9969.
58. Frolov,I., Hardy,R. and Rice,C.M. (2001) Cis-acting RNA elements at the 5' end of Sindbis virus genome RNA regulate minus- and plus-strand RNA synthesis. *RNA*, **7**, 1638–1651.
59. Gorchakov,R., Hardy,R., Rice,C.M. and Frolov,I. (2004) Selection of functional 5′ cis-acting elements promoting efficient Sindbis virus genome replication. *J. Virol.*, **78**, 61–75.
60. Hardy,R.W. (2006) The role of the 3′ terminus of the Sindbis virus genome in minus-strand initiation site selection. *Virology*, **345**, 520–531.
61. Hardy,R.W. and Rice,C.M. (2005) Requirements at the 3' end of the Sindbis virus genome for efficient synthesis of minus-strand RNA. *J. Virol.*, **79**, 4630–4639.
62. Spuul,P., Balistreri,G., Hellström,K., Golubtsov,A.V., Jokitalo,E. and Ahola,T. (2011) Assembly of alphavirus replication complexes from RNA and protein components in a novel trans-replication system in mammalian cells. *J. Virol.*, **85**:4739–4751.
63. Imataka,H., Gradi,A. and Sonenberg,N. (1998) A newly identified N-terminal amino acid sequence of human eIF4G binds poly(A)-binding protein and functions in poly(A)-dependent translation. *EMBO J.*, **17**, 7480–7489.
64. Wells,S.E., Hillner,P.E., Vale,R.D. and Sachs,A.B. (1998) Circularization of mRNA by eukaryotic translation initiation factors. *Mol. Cell*, **2**, 135–140.
65. Lloyd,R.E. (2013) Regulation of stress granules and P-bodies during RNA virus infection. *Wiley Interdiscip. Rev. RNA*, **4**, 317–331.
66. Lloyd,R.E. (2012) How do viruses interact with stress-associated RNA granules? *PLoS Pathog.*, **8**, e1002741.
67. Li,W., Li,Y., Kedersha,N., Anderson,P., Emara,M., Swiderek,K.M., Moreno,G.T. and Brinton,M.A. (2002) Cell proteins TIA-1 and TIAR interact with the 3' stem-loop of the West Nile virus complementary minus-strand RNA and facilitate virus replication. *J. Virol.*, **76**, 11989–12000.
68. Albornoz,A., Carletti,T., Corazza,G. and Marcello,A. (2014) The stress granule component TIA-1 binds tick-borne encephalitis virus RNA and is recruited to perinuclear sites of viral replication to inhibit viral translation. *J. Virol.*, **88**, 6611–6622.
69. Mackenzie-Liu,D., Sokoloski,K.J., Purdy,S. and Hardy,R.W. (2018) Encapsidated host factors in alphavirus particles influence midgut infection of Aedes aegypti. *Viruses*, **10**, 263.

Received: June 24, 2024. **Revised:** November 15, 2024. **Editorial Decision:** November 25, 2024. **Accepted:** November 29, 2024